JOURNAL OF GEOPHYSICAL RESEARCH, VOL. 103, NO. B5, PAGES 9691–9712, MAY 10, 1998

Quantitative measure of the variation in fault rheology due to fluid-rock interactions

M. L. Blanpied,[1] C. J. Marone,[2] D. A. Lockner,[1] J. D. Byerlee,[1] and D. P. King[2]

Abstract. We analyze friction data from two published suites of laboratory tests on granite in order to explore and quantify the effects of temperature (T) and pore water pressure (P_p) on the sliding behavior of faults. Rate-stepping sliding tests were performed on laboratory faults in granite containing "gouge" (granite powder), both dry at 23° to 845°C [*Lockner et al.*, 1986], and wet (P_p = 100 MPa) at 23° to 600°C [*Blanpied et al.*, 1991, 1995]. Imposed slip velocities (V) ranged from 0.01 to 5.5 μm/s, and effective normal stresses were near 400 MPa. For dried granite at all temperatures, and wet granite below ~300°C, the coefficient of friction (μ) shows low sensitivity to V, T, and P_p. For wet granite above ~350°, μ drops rapidly with increasing T and shows a strong, positive rate dependence and protracted strength transients following steps in V, presumably reflecting the activity of a water-aided deformation process. By inverting strength data from velocity stepping tests we determined values for parameters in three formulations of a rate- and state-dependent constitutive law. One or two state variables were used to represent slip history effects. Each velocity step yielded an independent set of values for the nominal friction level, five constitutive parameters (transient parameters a, b_1, and b_2 and characteristic displacements D_{c1} and D_{c2}), and the velocity dependence of steady state friction $\partial\mu_{SS}/\partial \ln V = a\text{-}b_1\text{-}b_2$. Below 250°, data from dry and most wet tests are adequately modeled by using the "slip law" [*Ruina*, 1983] and one state variable (a = 0.003 to 0.018, b = 0.001 to +0.018, $D_c \approx$ 1 to 20 μm). Dried tests above 250° can also be fitted with one state variable. In contrast, wet tests above 350° require higher direct rate dependence (a = 0.03 to 0.12), plus a second state variable with large, negative amplitude (b_2 = –0.03 to –0.14) and large characteristic displacement (D_{c2} = 300 to >4000 μm). Thus the parameters a, b_1, and b_2 for wet granite show a pronounced change in their temperature dependence in the range 270° to 350°C, which may reflect a change in underlying deformation mechanism. We quantify the trends in parameter values from 25° to 600°C by piecewise linear regressions, which provide a straightforward means to incorporate the full constitutive response of granite into numerical models of fault slip. The modeling results suggest that the succeptibility for unstable (stick-slip) sliding is maximized between 90° and 360°C, in agreement with laboratory observations and consistent with the depth range of earthquakes on mature faults in the continental crust.

1. Introduction

This study explores the effects of temperature, T, and pore water pressure, P_p, on the values of friction constitutive parameters for granite gouge. Fault slip at upper crustal and midcrustal depths occurs at elevated temperature and likely also with elevated pressures of aqueous pore fluids, i.e., hydrothermal conditions. Several physical and chemical processes may be accelerated or activated at these conditions, including accelerated crack growth, crack healing, retrograde mineral reactions, solution-transport creep, and hydrolytic weakening [e.g., *Tullis and Yund*, 1980]. Recent sliding experiments on laboratory faults in granite demonstrate that hydrothermal conditions can affect both frictional strength and the stability of sliding [*Blanpiedet al.*, 1991, 1992, 1995].

Models of fault slip and earthquake cycles employ a constitutive law to represent the frictional properties of the fault. Considerable use has been made of a class of empirical, rate- and state-dependent friction constitutive laws [*Dieterich*, 1978, 1979]. These laws describe the dependence of frictional strength on sliding velocity and recent sliding history and reproduce phenomena observed in studies of natural and laboratory faults, including time-dependent strengthening, stick slip, and oscillatory slip. They have been used to model earthquake cyclicity [*Tse and Rice*, 1986; *Stuart*, 1988], earthquake nucleation [*Dieterich*, 1986], postseismic slip [*Marone et al.*, 1991], and seismicity [*Dieterich*, 1994; *Ben-Zion and Rice*, 1995].

In modeling earthquake cycles on crustal-scale faults the parameters in the friction law are typically assigned values measured in (or extrapolated from) laboratory rock friction tests. A substantial body of literature exists on the frictional properties of rocks at room temperature. Few laboratory studies have been performed at hypocentral conditions, especially at the hydrothermal conditions thought to exist in the nucleation region of large earthquakes. However, sufficient data do exist to provide improved parameter values for slip at these conditions. In this paper we analyze previously published data from sliding tests on granite over a wide range of temperatures and both with and without elevated pore water pressure. We also evaluate three forms of the rate- and state-dependent friction constitutive law.

[1]Earthquake Hazards Team, U. S. Geological Survey, Menlo Park, California.

[2]Department of Earth, Atmospheric and Planetary Sciences, Massachusetts Institute of Technology, Cambridge.

Paper number 98JB00162.
0148-0227/98/98JB-00162/$09.00

On the basis of our inspection of friction-displacement curves we expect significant trends in the values of constitutive parameters as a function of temperature. *Lockner et al.* [1986] measured the velocity dependence of friction, the magnitude of the direct friction response, and the displacement persistence of the transient response for dry granite gouge. Each measurement showed systematic variation with temperature. *Blanpied et al.* [1991] similarly measured the velocity dependence for wet granite gouge and found a much stronger effect of temperature than that for the dry gouges of *Lockner et al.* [1986] or *Stesky* [1975, 1978]. We lack a detailed understanding of the physical and chemical processes that underlie the frictional velocity response and its dependence on temperature, and thus also of the link between each constitutive parameter and the microprocesses that determine its magnitude. However, the underlying, thermally activated processes are presumably subcritical crack growth, crystal plasticity, diffusion, and/or fluid-mineral reactions. If constitutive parameters are linked to the rate of thermally activated processes, linear trends may appear if we plot parameter values against inverse temperature. On such a plot, distinct changes of slope may indicate conditions at which the underlying process, or its rate-limiting step, changes, as is the case on conventional Arrhenius diagrams. Regimes and regime boundaries determined in this way are, of course, empirical. However, insight gained may help in the application of laboratory friction data in models of natural faulting and may provide guidance for future experimentation.

First we present the experimental data sets, followed by the constitutive formulations and the methods used to obtain parameter values. Results of the analysis are followed by a discussion of implications for the stability of fault slip.

1.1. Experimental Data

Experimental results from two studies [*Lockner et al.*, 1986; *Blanpied et al.*, 1991, 1995] form the basis of the analysis presented below. In both studies, slip rate-stepping tests were performed in a triaxial gas apparatus on cylindrical samples of Westerly granite. "Faults" consisted of a saw cut separated by a thin layer (~0.6 mm) of simulated fault gouge (granite powder, particle sizes of ≤90 μm). *Lockner et al.* [1986] performed tests on predried samples ("dry") at constant temperatures ranging from 23° to 845°C. Confining pressure was maintained at 250 MPa, resulting in normal stresses (resolved across the sawcut) in the range 400 to 460 MPa during the velocity-stepping portion of the tests. *Blanpied et al.* [1991, 1995] added a constant pore water pressure of 100 MPa ("wet"). Temperatures ranged from 23° to 600°C, and effective normal stress ($\sigma_n = \sigma_n - P_p$) was maintained constant at 400 MPa by adjusting the confining pressure. In both studies the shortening rate was periodically stepped by factors of 10. Slip rates in the dry tests, resolved onto the sawcut, were 0.055, 0.55, and 5.5 μm/s. Slip rates in the wet tests alternated either between 0.1 and 1.0 μm/s or between 0.01 and 0.1 μm/s. Other than the differences noted here the dry and wet suites of experiments were nominally identical. Experiments were terminated by rupture of sample jackets, typically after 3 to 4 mm of axial shortening and 2 to 3 mm slip on the fault. Samples were examined by optical microscopy and, in a few cases, scanning electron microscopy. Fluid chemistry was not analyzed.

Figures 1 and 2 show representative friction-displacement curves from the dry and wet suites of experiments, respectively. Strength variations resulting from the velocity steps indicated at the top of each figure are superimposed on longer-term work-hardening or work-softening trends. Each velocity step resulted in an immediate change of friction in the same sense as the velocity

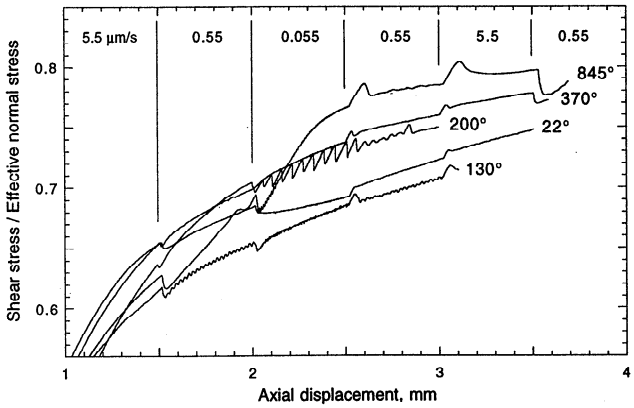

Figure 1. Representative friction–displacement curves from *Lockner et al.* [1986] for dry granite "gouge." Runs were performed on predried, vented samples, at a constant confining pressure of 250 MPa. Shortening rate was stepped, as noted at the top of the figure. Short-period oscillations in some runs (most notably at 130°) are due to small fluctuations in temperature.

change (the "direct effect"), followed by an evolution of friction to a new level relative to the longer-term trend. In tests on wet granite at the higher temperatures there was insufficient slip between steps for the rate step-induced evolution to conclude. For purposes of modeling with friction constitutive laws presented below it is convenient to regard the behavior following a rate step to reflect a disturbance and subsequent evolution to a new steady state friction value, despite this "steady state" actually consisting of a hardening or softening trend.

Two distinct regimes exist (Figures 1, 2, and 3): The first regime includes dry granite at all temperatures and wet granite below 250°. Friction coefficients fall in the range $\mu = 0.7$ to 0.8, in agreement with results for many rock materials at room temperature [*Byerlee*, 1978], and frictional strength is fairly insensitive to temperature, slip velocity, and P_p. The strength transients following velocity steps are small in amplitude, and the steady state trend is generally reestablished after ~50 to 200 μm further slip. The second regime includes wet granite above ~350°, where strength decreases with increasing temperature and varies strongly with slip velocity. Velocity steps are followed by protracted strength transients of large amplitude. *Blanpied et al.* [1991, 1995] inferred that one or more unspecified fluid-activated deformation processes were active in this second regime. Shearing tests on quartzite powder at hydrothermal conditions, accompanied by microstructural evidence [*Higgs*, 1981; *Chester and Higgs*, 1992], show that solution-transport of silica can accompany cataclasis at conditions similar to those in the second, hydrothermal, regime. Thus solution-transport creep in quartz is one candidate mechanism to explain the reduced strength at hydrothermal conditions. Other candidates include acceleration of subcritical crack growth rates and incongruent pressure solution of feldspars involving the production of phyllosilicate minerals [*Blanpied et al.*, 1995].

1.2. Constitutive Formulation

We analyze the experimental results in the context of three widely used, rate- and state-dependent friction constitutive laws, each based on laws originally formulated by *Dieterich* [1978, 1979]. The empirical law is based on experimental observations, such as those in Figures 1 and 2, which show that frictional resistance depends both on slip velocity and on the recent history of velocity:

$$\tau = \mu \cdot \bar{\sigma}_n, \quad \mu = f(V, \text{past } V) \tag{1}$$

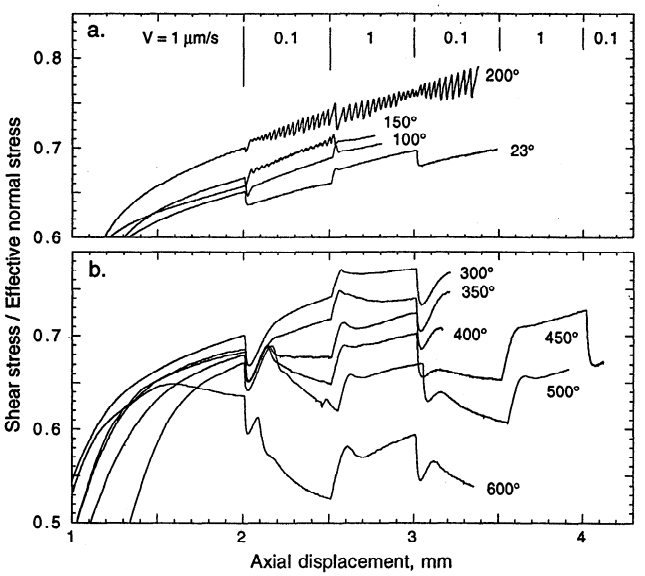

Figure 2. Representative friction–displacement curves from *Blanpied et al.* [1991, 1995] for H_2O–saturated granite "gouge." Conditions are effective normal stress, 400 Mpa; and P_p = 100 MPa.

The coefficient of friction can be written as

$$\mu = \mu_* + a\ln\left(\frac{V}{V_*}\right) + b_1 \ln\left(\frac{V_*\theta_1}{D_{c1}}\right) + b_2 \ln\left(\frac{V_*\theta_2}{D_{c2}}\right) \qquad (2)$$

where V is instantaneous sliding velocity resolved along the saw-cut, θ_1 and θ_2 are "state variables" that parameterize the evolving state of the sliding surface and reflect history-dependent processes, D_{c1} and D_{c2} are characterisitic displacements scaling the evolution of the state variables (see below), and μ_* and V_* are constants. Scaling parameters a, b_1, and b_2 are generally measured to be on the order of 10^{-2}. Thus μ_* identifies a reference, nominal coefficient of friction, and the following terms are second-order contributions. The second term in (2) describes the direct change of friction in response to changes in slip rate, and the following terms describe the evolution of state affects friction. Analysis of laboratory rock friction data has shown that one or two state variables are usually sufficient to represent the response of friction to velocity steps.

The second term in (2) acts as an instananeous viscosity, which *Dieterich* [1978, 1979] interprets to result from a rate dependence of sliding resistance at asperity contacts. This interpretation allows one to view the direct effect (the instantaneous response of friction to slip rate, scaled by a) as representing a deformation mechanism. Two studies have attributed deformation mechanisms to the direct effect. *Reinen et al.* [1992] measured a velocity dependence but no sliding-history dependence for serpentinite surfaces slid at low rates. They argued that the direct effect in this case is dislocation glide. *Lockner* [1988] has shown that the constitutive law (2) can be derived from relations describing deformation by subcritical crack growth. Furthermore, he measured a = 0.008 in fracture tests on intact granite, consistent with values measured in numerous sliding studies of both bare granite surfaces and granite gouge.

1.3. Friction State Dependence

The state variables θ_1 and θ_2 evolve with displacement or with time to reflect the evolution of state in response to changing slip

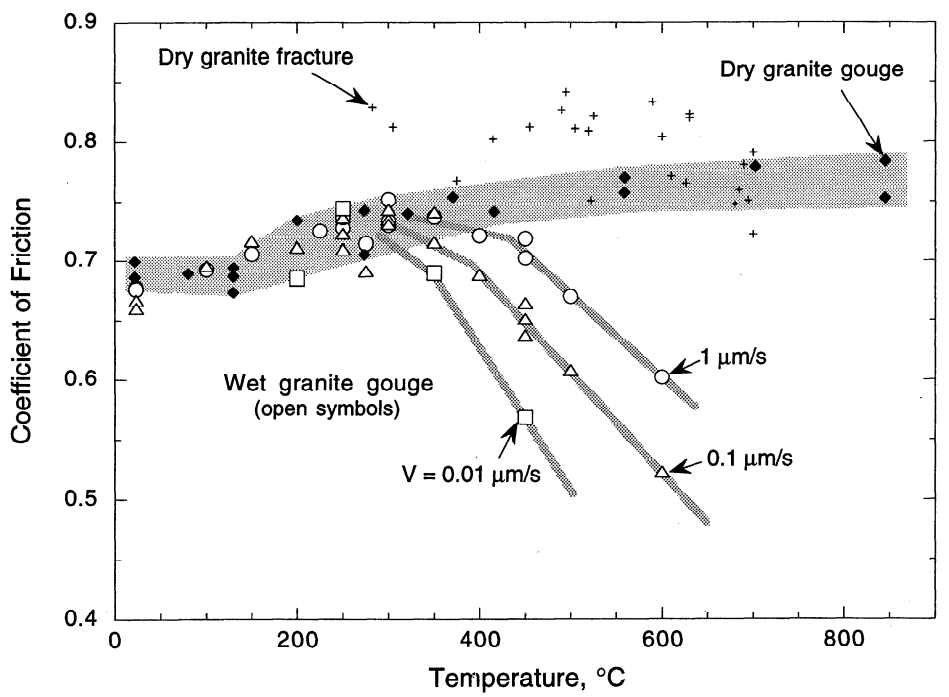

Figure 3. Friction measured at 2.9 mm axial displacement (shortening) versus temperature. Values for wet granite gouge from *Blanpied et al.* [1995] (open symbols for three slip rates as labeled, 400 MPa effective normal stress), for dry granite gouge from *Lockner et al.* [1986, Figure 5] (closed diamonds, σ_n = 380 to 460 MPa), and from sliding tests on dry, prefractured granite from *Stesky* [1975] (dots, σ_n = 370 to 450 MPa). Ambiguities in the strength measurements for wet gouge are generally less than the symbol size. Values for wet and dry gouges have been corrected for the temperature-dependent strength contribution from the copper sample jackets. Gray shading and gray lines are visual guides to indicate the trend in values for dry gouge and for wet gouge, respectively, at three slip rates. Figure from *Blanpied et al.* [1995].

rate. Identifying the physical and/or chemical processes responsible for the evolution of state has been challenging. Various theories have linked state to the size distribution of load-bearing points of contact between surfaces [*Dieterich*, 1978; *Dieterich and Kilgore*, 1994] or within a gouge layer [*Dieterich*, 1981; *Biegel et al.*, 1989], to compaction and dilation of the gouge [*Morrow and Byerlee*, 1989; *Marone et al.*, 1990; *Marone and Kilgore*, 1993], or to the chemical forces acting at points of contact [*Tullis*, 1994]. *Dieterich and Kilgore* [1994] directly observed the distribution of contact points between bare surfaces of transparent materials. They linked the evolution of friction following slip rate steps to the displacement-dependent replacement of the contact population. In their model the characteristic displacement D_c scales with the mean diameter of the contact points. *Marone and Kilgore* [1993] sheared layers of granite powder (gouge), observing the way gouge layer thickness evolves in response to slip rate steps. They showed D_c to scale with shear strain and argued that D_c for gouge is controlled by the width of the actively deforming shear zone within the gouge; thus the evolution of state quantifies changes in shear zone width in response to slip rate steps. Published theories rarely attempt to explain why two state variables are often required to accurately model laboratory data.

We examine two of the several equations that have been proposed to characterize the evolution of state (see *Linker and Dieterich* [1992 and *Beeler et al.* [1994] for further discussion of evolution laws). The first, proposed by *Ruina* [1983], has been widely employed to model velocity-stepping friction experiments and earthquake cyclicity. It can be written

$$\frac{\partial\theta_i}{\partial t} = -\left(\frac{V\theta_i}{D_{ci}}\right)\ln\left(\frac{V\theta_i}{D_{ci}}\right), \quad (i=1,2) \tag{3}$$

where D_{ci} are characteristic displacements over which the state variables evolve. Following convention, we apply subscript "1" to the state variable with the shorter characteristic displacement (i.e., $D_{c1} < D_{c2}$). For convenience, we will refer to the combination of constitutive equation (2) and evolution law (3) as the "slip law" because (3) requires that slip occur in order for state to evolve (i.e., surfaces in stationary contact do not strengthen). Despite its usefulness in modeling data, (2) has no direct physical interpretation linking it to the micromechanics of the sliding process.

The second equation has been used principally by Dieterich and coworkers and can be written

$$\frac{\partial\theta_i}{\partial t} = 1-\left(\frac{V\theta_i}{D_{ci}}\right), \quad (i=1,2) \tag{4}$$

This evolution law is superior to (3) in modeling the changes in friction during slide-hold-slide (stress relaxation) tests [*Beeler et al.*, 1994] and normal stress stepping tests [*Linker and Dieterich*, 1992]. However, it is not "symmetric"; i.e., the response to a velocity increase is not the mirror image of that to a velocity decrease. As data from laboratory velocity-stepping experiments are often symmetric or nearly so, this equation often provides an inferior match to those data in comparison with (3). In contrast to the slip law, the term "1" in (4) allows for restrengthening ("aging") at low velocity or truly stationary contact, as observed in laboratory slide-hold-slide tests (see *Beeler et al.*, 1994). Equation (4) can be directly linked to the physics of sliding. For example, *Sleep* [1995] derives its form considering state to represent gouge porosity and the terms on the right-hand side of (4), reflecting competition between porosity loss through creep at low or zero velocity versus porosity generation through cracking at high velocity. We will refer to the combination of constitutive equation (2) and evolution law (4) as the "slowness law," because at steady state, state is proportional to slowness V^{-1}, i.e., $(\theta_i)_{ss} = D_c/V$ [*Ruina*, 1983].

An alternate form of the constitutive law has more recently been proposed by *Perrin et al.* [1995]:

$$\mu = \mu_* + a\ln\left(\frac{V}{V_*}\right) + b_1\ln\left(\frac{V_*\theta_1}{2D_{c1}}\right) + b_2\ln\left(\frac{V_*\theta_2}{2D_{c2}}\right) \tag{5}$$

$$\frac{\partial\theta_i}{\partial t} = 1-\left(\frac{V\theta_i}{2D_{ci}}\right)^2, \quad (i=1,2) \tag{6}$$

This formulation gives similar results to the slip law in simulations of velocity step response, and, like the slip law, gives symmetric, mirror-image responses for increasing and decreasing velocity steps. Like the slowness law, evolution law (6) allows restrengthening during stationary contact. We will refer to the combination of (5) and (6) as the "quadratic law."

At steady state, by definition, $\partial\theta_1/\partial t = \partial\theta_2/\partial t = 0$. Setting the right side of evolution law (3), (4), or (6) equal to zero, solving for θ_i and substituting into (1) yields

$$\mu_{ss} = (a-b_1-b_2)\ln\left(\frac{V}{V_*}\right) \tag{7}$$

where μ_{ss} is the steady state coefficient of friction at velocity V. The velocity dependence of steady state friction is thus measured by the quantity $(a\text{-}b_1\text{-}b_2)$:

$$\frac{\partial\mu_{ss}}{\partial\ln V} = (a-b_1-b_2). \tag{8}$$

In many cases it is found that laboratory data are adequately described by a constitutive law with only a single state variable. In this case the last term of (2) is omitted (or equivalently, b_2 can be set to zero), and the steady state velocity dependence is simply written $a\text{-}b$. In many papers the rather cumbersome term $a\text{-}b_1\text{-}b_2$ is often written simply as $a\text{-}b$, for example, when the number of state variables required to model the data is unknown or unstated, or when only the net velocity dependence is of interest.

To model laboratory data, the constitutive law (2) and an evolution equation (3) or (4) (or the *Perrin et al.* [1995] equations (5) and (6)) are coupled with an equation describing the compliant coupling between the frictional surface and its surroundings. For the geometry of the triaxial friction test, elastic interactions are adequately described by the time derivative of a simple spring equation:

$$\frac{d\mu}{dt} = K(V_o - V) \tag{9}$$

where V_0 is the remote velocity measured at the displacement control point and K is stiffness in units of coefficient of friction per displacement. For our modeling of data from triaxial sliding tests we resolve displacement parallel to the inclined slip vector. K was measured from the loading slope that immediately follows upward velocity steps, and varies somewhat between experiments. The source of this variation is unclear. For runs with constant confining pressure, K ranged from 0.27 to 0.31/mm. For

runs with constant normal stress, K ranged from 0.62 to 0.81/mm (these values are higher because the adjustment of confining pressure used to servo-control normal stress increases the apparent stiffness of the experimental system). An independent value of K was determined for each experiment and used for all inversions involving those data.

None of the three constitutive laws used here contains temperature as a variable. Therefore the variation of parameter values with temperature is revealed by comparing values determined at different temperatures. In this context the parameters are not material constants but are themselves functions of temperature. A different approach has been used by *Chester* [1988, 1994] and *Chester and Higgs* [1992], who incorporated temperature into the constitutive and evolution equations, thereby expressing temperature dependence explicitly. Parameters in Chester's constitutive law are best determined through a matrix of velocity-stepping and temperature-stepping experiments [*Chester*, 1994]. Abrupt temperature steps on laboratory faults are difficult to impose at high temperatures, and the requisite data are not yet available over the range of conditions of interest here. *Blanpied et al.* [1995] analyzed the steady state friction values from Figure 3 in the context of Chester's formulation.

1.4. Analysis Technique

We inverted the experimental data to obtain values for each of the constitutive parameters a, b_1, b_2, D_{c1}, and D_{c2}, plus μ_{ss} at the prior velocity, for a total of six unknown parameters. We used an iterative, least squares method to solve the nonlinear inverse problem. In this approach one starts with a model vector **a** containing initial estimates of the unknowns and calculates a correction vector **m** by solving the linearized inverse problem:

$$\mathbf{G\,m = d}, \tag{10}$$

where G_{ij} is a matrix of partial derivatives $\partial\mu_i/\partial a_j$ and d_i is the residuals vector $d_i = \mu_i^{obs} - \mu_i^{pred}$ of differences between friction observations and model predictions. Following *Reinen and Weeks* [1993], we imposed positivity constraints on D_{c1} and D_{c2} by solving for their logarithms. In addition, we weighted data nearest to the velocity step, using a weighting vector $W_i = (Ni)^c$, where N is the size of the data vector and i is an index incremented from a value of 1 at the velocity step. We tried values of the exponent c from 0 to 2 and found that $c = 1$ worked best for our data. This value was used in all the modeling reported here. (Note that *Reinen and Weeks* [1993] used a similar weighting scheme with $c = 2$.)

We used singular value decomposition of **G** [*Press et al.*, 1988; *Menke*, 1989] to solve the weighted, least squares linearized inverse problem:

$$\mathbf{m} = (G^T W^T W G)^{-1} G^T W^T W d \tag{11}$$

Our method is similar to that of *Reinen and Weeks* [1993], except that we exploy a true Levenberg-Marquardt method (variable damping) in the inversion, whereas they use a fixed damping parameter λ. We generally began the inversions with $\lambda = 0.1$. Following *Reinen and Weeks* [1993], we calculate the numerical partial derivatives in **G** for only a small fraction of the model space spanned by the components of **m**. In addition, after the solution converged, we set $\lambda = 0$ when calculating the covariance matrix C_{jk} and model variance. Following standard techniques [*Menke*, 1989], our covariance matrix includes the data variance σ:

$$C_{jk} = \sigma^2 (G_{ij}^T W_i^T W_i G_{ij})^{-1} \tag{12}$$

$$\sigma^2 = \sum_{i=1}^{N} \left(\frac{(\mu_i^{obs} - \mu_i^{pred}}{N - M} \right) \tag{13}$$

where M is the number of model parameters (six in this case). Because N is generally a large number for our inversions (artificially large with respect to parameter resolution), the resulting covariance estimates and standard deviations are artificially low, as we discuss below. In some cases the solution converged to a degenerate, one state variable model ($b_2 = 0$, or $D_{c1} = D_{c2}$) fit.

Certain pairs or combinations of constitutive parameters have a strong covariance. Figure 4 shows data from an upward velocity step (solid circles). The solid curve is the best fit obtained by nonlinear least squares inversion to the 157 points shown. Table 1 lists the covariance between each pair of parameters obtained in the inversion, as well as the correlation coefficients, which can range from 1 (perfect correlation) to –1 (perfect anticorrelation). The correlation coefficient for a and b_1 is over 0.99 in this example, indicating that the values of a and b_1 are poorly determined in relation to their difference a-b_1. In other words, the best fit is only slightly superior to a fit in which both a and b_1 are both, say, increased by equal amounts (Figure 4, short-dashed line). The three remaining curves in Figure 4 illustrate the effect of changing the values of other highly correlated parameters. In later figures and tables we report a magnitude of error associated with each parameter value calculated as the standard deviation (square root of the covariance of a parameter with itself). Because we invert for log D_c rather than D_c, covariances are for log D_c. The standard deviation of D_{c1} and D_{c2} is then +exp(log D_c +(cov.)$^{-1}$) – exp(log D_c) and –exp(log D_c –(cov.)$^{-1}$) – exp(log D_c). We quote the larger of these values as the standard deviation. Error from additional sources is not represented by the standard deviation. These sources include the off-diagonal terms of the covariance matrix (Table 1), as well as others discussed below. The effects of parameter correlations are discussed further by *Reinen and Weeks* [1993].

Most of the run records in Figures 1 and 2 display long-term displacement hardening or softening. We assume that these trends reflect the evolution of gouge microstructure with increasing displacement and are largely unrelated to the transient effects of velocity steps (see discussions by *Lockner et al.* [1986], *Tullis and Weeks* [1986], *Marone et al.* [1990], *Chester* [1994], and *Beeler et al.* [1996]). We accounted for these trends by adding the term $C\delta$ to the constitutive equations for μ, (2) and (5), where δ is displacement and C scales a linear trend determined by inspection of the data. Further details are given in the appendix.

The response to a given change of velocity varies from step to step even in a single experiment. Two strategies were adopted in our analysis. The first was to analyze the response to each velocity step independently, yielding a separate set of parameter values for each step and up to several independent sets of parameters (one set per velocity step) at each set of conditions (temperature, pore pressure, velocity interval). This method allows each step to be fitted closely, but the resulting parameter values may show scatter even at fixed conditions. The second stretegy was to invert the data from an entire experiment for a single set of parameter values. In this case the responses to individual steps are not fitted

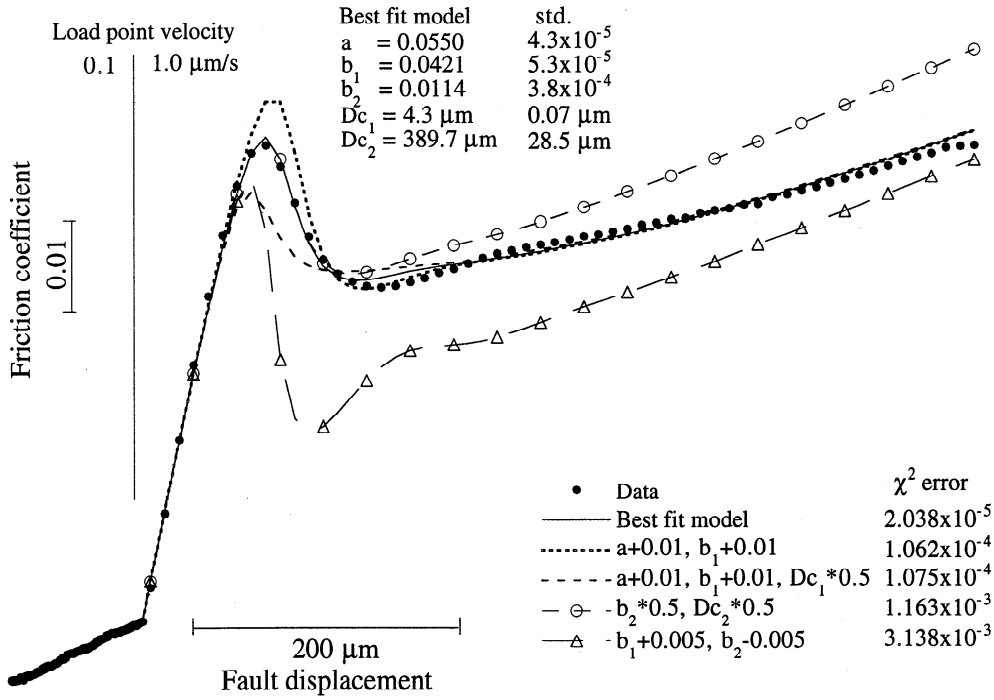

Figure 4. Experimental data (solid circles) showing the response of friction to a ten-fold increase in shortening rate (run at 600°, P_p = 10 MPa). The displacement axis in this plot and following ones is sample shortening expressed in units of slip on the inclined sawcut. Five simulations using the slip law (2) are shown as solid and dashed curves. The solid curve is the best fit model obtained by nonlinear least squares inversion to the 157 points shown. The parameter values for this fit are shown at the top of the figure. The four remaining curves illustrate the effect of changing the values of two or three highly correlated parameters. For example, raising both a and b_1 by 0.01 (short dashes) raises the transient peak height, while halving D_{c1} (medium dashes) lowers the initial peak and decreases the rate of evolution toward steady state.

as well, but a single "representative" value for each parameter is determined for each set of conditions. We show results obtained by using both methods.

2. Application of Methods and Inversion Results

2.1. Fits to Individual Velocity Steps

We first present results that were obtained by analyzing each velocity step individually (Tables 2 and 3). Data are compared to best fit simulations by using the slip law (3) in Figures 5 and 6 for dry and wet experiments, respectively. In each case the major features of the data are fairly well matched by the simulation. Most steps for dry gouge were fitted adequately with a single state variable with D_{c1} < 100 μm, although the addition of a second state variable with small amplitude ($|b_2| < |b_1|$) noticeably improved the fit in some cases. Similarly, for wet granite below 250° one state variable was generally sufficient to obtain a good fit. However, wet granite at higher temperatures required two state variables: The protracted evolution of strength seen in runs

Table 1. Variance and Correlation Parameters of the Best Fitting Model of Figure 5

	μ	a	b_1	D_{c1}	b_2	D_{c2}
			Covariance Matrix[a]			
μ	1.3063x10-9					
a	-1.1371x10-10	1.8470x10-9				
b_1	1.0057x10-10	-2.2503x10-9	2.7843x10-9			
D_{c1}	-4.1401x10-8	-4.9584x10-7	6.2269x10-7	2.6286x10-4		
b_2	-3.1523x10-10	-9.1596x10-9	1.3156x10-8	2.6293x10-6	1.4449x10-7	
D_{c2}	-1.2219x10-7	-2.3430x10-6	3.1426x10-6	6.6809x10-4	2.5556x10-5	4.9911x10-3
			Correlation Coefficient Matrix			
μ	1.0000					
a	-0.0732	1.0000				
b_1	0.0527	-0.9923	1.0000			
D_{c1}	-0.0707	-0.7116	0.7279	1.0000		
b_2	-0.0229	-0.5607	0.6559	0.4266	1.0000	
D_{c2}	-0.0479	-0.7717	0.8430	0.5833	0.9517	1.0000

[a] Covariance scaled by the uniform variance (1.406x10-7) of the best fit model. Because we invert for logD_c rather than D_c, covariances are for logD_c. The standard deviation of D_{c1} and D_{c2} is then +exp(logD_c +(cov.)$^{-1}$)–exp(logD_c) and –exp(logD_c –(cov.)$^{-1}$)–exp(logD_c). We use the larger of these values as the standard deviation.

Table 2. Parameter Values Determined by Inversion by Using the Slip Law, Equations (2) and (3)

T, °C	Disp.[a], mm	μ	μ s.d. x10^{-4}	a x10^{-2}	a s.d. x10^{-4}	b_1 x10^{-2}	b_1 s.d. x10^{-4}	D_{c1}, μm	D_{c1} s.d.	b_1 x10^{-2}	b_2 s.d., x10^{-4}	D_{c2}, μm	D_{c2} s.d.	$a-b_1-b_2$ x10^{-2}
							Wet runs[b]							
23	2.0	0.6515	0.36	0.79	0.79	0.10	0.72	19.84	1.57					0.687
	2.5	0.6610	0.12	1.05	5.94	0.53	5.62	4.92	0.81	-0.14	0.73	127.4	17.7	0.657
	3.0	0.6971	0.38	1.46	0.09	0.70	0.09	3.90	0.14					0.759
100	2.0	0.6577	0.39	1.61	5.42	1.34	5.23	4.01	0.18	0.40	0.25	150.2	2.8	-0.133
	2.5	0.6895	0.09	1.11	5.79	0.83	5.40	3.35	0.34	0.46	2.11	182.4	20.9	-0.181
150	2.0	0.6670	1.10	1.39	8.13	1.37	7.45	2.86	0.19	0.44	0.70	106.8	3.6	-0.428
250	2.0	0.6849	1.30	1.41	0.36	0.50	0.37	2.45	0.87	1.28	5.08	565.7	38.5	-0.367
	2.5	0.7176	1.07	1.25	0.89	0.48	1.18	1.55	2.21	1.53	55.48	908.4	568.4	-0.755
	3.0	0.7545	2.14	1.80	0.68	0.50	1.03	8.60	2.41	1.50	11.32	559.5	79.7	-0.203
300	2.0	0.6781	0.61	2.81	2.6	2.09	3.09	40.36	1.36	0.87	3.44	213.8	16.1	-0.139
350	2.0	0.6810	0.58	3.09	2.87	2.24	3.95	27.14	0.91	1.10	5.68	89.2	2.6	-0.253
	2.5	0.7184	0.35	3.89	0.27	2.76	0.28	1.69	0.06	1.97	2.30	443.7	11.0	-0.842
	3.0	0.7404	0.92	3.78	3.41	0.66	1.23	27.43	2.46	2.97	1.27	32.1	1.1	0.149
400	2.0	0.6851	3.04	4.33	14.16	4.16	11.87	17.48	0.70	-3.03	61.59	1255.0	386.6	3.191
	2.5	0.6779	0.40	3.04	16.31	1.91	15.89	11.10	1.27	-5.21	23.53	2806.0	111.3	6.336
500	2.0	0.6734	6.99	3.11	13.37	4.17	5.69	39.97	2.40	-10.54	397.71	1499.0	925.6	9.478
	2.5	0.6198	0.98	4.53	0.28	3.12	0.30	4.57	0.08	-4.94	3.37	4348.0	30.0	6.356
	3.0	0.6710	0.64	9.38	3.86	8.27	4.36	6.82	0.05	-13.66	175.80	2892.0	439.0	14.778
	3.5	0.6073	3.44	3.70	36.29	2.00	34.58	10.03	2.36	-4.50	74.14	4178.0	612.9	6.197
600	2.0	0.6372	4.42	11.31	0.99	11.00	1.04	5.44	0.08	-5.51	4.97	298.4	7.8	5.817
	2.5	0.5266	3.02	5.04	30.64	3.50	29.25	13.32	1.54	-9.76	52.77	2904.0	145.1	11.310
	3.0	0.5960	5.15	11.59	1.18	10.52	2.64	7.88	0.21	-2.84	47.45	589.4	172.1	3.906
600[c]	2.0	0.7288	1.58	3.53	6.14	2.60	3.66	36.86	1.67	0.26	1.74	348.9	254.2	0.660
	2.5	0.7491	0.36	5.50	0.43	4.21	0.53	4.31	0.07	1.14	3.80	389.7	28.5	0.148
	3.0	0.7974	3.29	6.01	28.60	4.83	19.31	25.64	2.46	0.46	4.10	259.8	176.9	0.717
250[d]	2.0	0.6944	0.34	4.69	0.20	3.32	0.22	6.88	0.06	1.84	0.34	148.5	0.6	-0.471
350[d]	2.0	0.7081	3.66	2.76	10.85	2.96	8.35	13.24	0.57	-0.72	27.80	800.5	636.8	0.520
	2.5	0.7074	1.96	2.12	68.38	1.40	68.09	5.97	4.51					0.716
	3.0	0.7475	2.82	3.41	17.38	3.20	15.03	12.94	0.87	-0.16	3.13	305.7	313.1	0.373
	3.5	0.7402	1.20	3.71	36.23	2.69	35.99	5.54	0.93					1.028
450[d]	2.0	0.6502	0.90	4.97	0.30	3.64	0.33	7.72	0.11	-3.41	1.17	349.1	3.5	4.743
	2.5	0.5569	0.77	4.08	28.24	2.42	28.10	7.83	1.14	-6.77	85.70	2852.0	405.9	8.428
							Dry runs[e]							
22	2.5	0.6923	0.28	0.92	0.19	0.68	0.19	1.13	0.08	-0.14	0.68	185.5	27.0	0.384
	3.0	0.7240	0.37	0.32	2.60	0.19	2.55	11.68	2.27					0.133
80	2.0	0.6683	0.81	0.52	1.88	0.37	1.73	24.39	1.37					0.149
	2.5	0.6877	0.34	0.73	3.62	0.46	3.23	6.09	0.72	0.19	0.48	111.5	7.7	0.076
200	2.7	0.7444	0.88	0.39	2.29	0.42	2.09	17.31	1.55					-0.030
370	2.0	0.7042	0.49	0.33	0.91	0.32	0.82	45.41	1.86					0.010
	2.5	0.7372	0.28	0.75	2.36	0.67	1.83	4.87	0.30	-0.21	0.81	44.1	1.8	0.286
	3.0	0.7597	0.31	0.56	4.67	0.35	4.63	6.48	1.11					0.208
416	2.5	0.7191	0.48	0.68	4.03	0.72	2.38	4.46	0.59	-0.31	3.66	23.4	2.3	0.273
559	2.0	0.7115	1.37	1.29	5.97	1.14	16.61	3.76	1.84	-0.14	22.16	23.6	61.8	0.290
	2.5	0.7433	1.90	0.60	3.78	0.27	2.30	54.24	17.80	0.19	6.08	494.5	57.0	0.151
	3.0	0.7581	0.64	1.00	2.27	0.71	0.73	65.70	5.25	0.36	4.07	250.3	41.6	-0.065
702	2.5	0.7664	1.11	1.35	13.25	0.99	9.78	9.33	2.44	-0.06	5.40	65.2	74.6	0.413
	3.0	0.7805	0.51	2.19	0.70	1.61	0.73	2.68	0.23	0.29	1.22	128.8	12.4	0.289
845	2.5	0.7681	1.36	1.67	12.00	1.38	11.65	9.15	1.03					0.289
	3.0	0.7855	0.44	1.59	14.08	1.00	13.27	8.17	1.65	0.63	0.84	213.4	10.7	-0.037
600[f]	2.0	0.7228	1.01	2.96	10.50	2.25	8.71	11.03	0.71	1.15	2.19	89.9	1.9	-0.438
	2.5	0.7737	1.38	4.10	1.12	3.60	1.20	1.70	0.12	0.90	10.58	451.1	120.9	-0.404
	3.0	0.7960	1.21	4.55	0.55	3.56	0.61	5.94	0.12	1.33	1.04	105.1	1.4	-0.347
	3.5	0.8134	1.16	5.30	0.74	4.80	0.87	1.87	0.06	0.60	16.37	646.2	356.7	-0.101

[a] Corresponding velocity steps were, for wet runs, 2.0 and 3.0 mm, 1 to 0.1 μm/s; 2.5 and 3.5 mm, 0.1 to 1 μm/s; and, for dry runs, 2.0 mm, 5.5 to 0.55 μm/s; 2.5 mm, 0.55 to 0.055 μm/s; 3.0 mm, 0.055 to 0.55 μm/s; 3.5 mm, 0.55 to 5.5 μm/s.

[b] For wet runs, pore pressure was 100 MPa, and constant normal stress was 400 Mpa.

[c] Pore pressure was 10 Mpa.

[d] Ten times slower slip rates were used.

[e] For dry runs, no pore fluid was used, and constant confining pressure was 250 MPa.

[f] Data from experimental suite at constant normal stress of 400 MPa.

Table 3. Parameter Values Determined by Inversion by Using the Slowness Law, Equations (2) and (4)

T, °C	Disp.[a], mm	μ	μ s.d. x10^{-4}	a x10^{-2}	a s.d. x10^{-4}	b_1 x10^{-2}	b_1 s.d. x10^{-4}	D_{c1}, mm	D_{c1} s.d.	b_1 x10^{-2}	b_2 s.d., x10^{-4}	D_{c2}, mm	D_{c2} s.d.	$a-b_1-b_2$ x10^{-2}
							Wet runs							
23	2.0	0.6515	0.37	0.79	0.81	0.10	0.73	29.86	3.03					0.686
	2.5	0.6610	0.12	1.03	5.81	0.51	5.62	3.54	0.47	-0.12	0.62	65.5	5.3	0.649
	3.0	0.6971	0.37	1.35	0.08	0.60	0.09	5.48	0.20					0.758
100	2.0	0.6578	0.31	2.01	0.15	1.68	0.16	2.84	0.04	0.52	0.22	357.2	8.9	-0.180
	2.5	0.6895	0.10	0.97	3.71	0.73	3.55	3.27	0.20	0.43	1.07	103.7	5.4	-0.197
150	2.0	0.6670	0.91	2.64	0.30	2.50	0.31	1.15	0.02	0.59	0.54	206.5	7.2	-0.447
250	2.0	0.6850	1.40	1.62	0.44	0.70	0.44	1.65	0.84	1.30	4.38	1615.0	134.2	-0.379
	2.5	0.7176	0.87	1.23	0.51	0.47	0.52	1.50	1.11	2.61	3.33	714.6	9.2	-1.852
	3.0	0.7548	2.75	1.60	0.85	0.30	3.66	20.52	12.25	2.00	19.42	2385.0	619.3	-0.702
300	2.0	0.6781	0.61	2.60	1.96	1.16	0.92	56.14	2.28	1.54	1.19	227.0	3.3	-0.092
350	2.0	0.6810	0.69	2.90	2.57	1.03	1.57	30.91	1.40	2.10	0.90	108.0	0.6	-0.230
	2.5	0.7184	0.31	3.47	0.22	2.37	0.22	1.90	0.05	1.49	0.68	149.5	1.6	-0.382
	3.0	0.7404	1.26	3.68	1.58	1.52	0.59	15.51	1.16	2.49	4.99	147.9	12.2	-0.326
400	2.0	0.6854	3.81	4.38	13.26	4.32	10.38	24.18	1.19	-2.22	18.75	2024.0	475.7	2.277
	2.5	0.6779	0.40	3.16	20.37	2.02	19.94	7.40	0.83	-3.35	12.92	760.9	24.8	4.498
500	2.0	0.6741	5.91	3.57	7.77	5.36	4.23	70.61	2.64	-8.40	13.79	2363.0	24.1	6.603
	2.5	0.6198	1.02	4.93	0.30	3.51	0.31	3.33	0.05	-4.42	3.46	1576.0	12.4	5.841
	3.0	0.6708	0.60	5.90	12.38	5.00	11.32	17.28	0.62	-7.83	30.84	4059.0	265.3	8.732
	3.5	0.6073	2.77	3.70	21.96	2.00	20.54	10.00	1.19	-4.51	30.30	2584.0	155.0	6.208
600	2.0	0.6377	4.46	18.58	0.94	18.14	1.01	3.67	0.05	-8.95	19.70	1647.0	75.3	9.396
	2.5	0.5266	3.29	5.29	42.98	3.71	41.31	9.01	1.16	-14.01	34.64	1809.0	33.0	15.597
	3.0	0.5964	5.10	16.78	1.33	15.62	2.80	5.62	0.14	-6.30	197.76	5383.0	2800.0	7.463
600[b]	2.0	0.7242	1.56	3.86	14.21	2.39	10.15	22.04	2.98	0.98	10.20	184.0	30.1	0.487
	2.5	0.7492	0.21	4.62	20.77	3.39	20.38	4.82	0.32	0.97	2.28	158.8	7.6	0.263
	3.0	0.7917	1.83	7.90	3.30	5.52	4.91	9.95	0.48	1.66	8.27	87.5	4.0	0.725
250[c]	2.0	0.6943	0.23	5.29	0.19	3.69	0.20	3.45	0.05	2.24	0.22	342.1	2.0	-0.644
350[c]	2.0	0.7089	5.14	3.50	17.27	3.51	15.54	11.36	0.63					-0.005
	2.5	0.7074	1.96	2.10	72.13	1.39	71.86	4.58	3.04					0.715
	3.0	0.7478	2.34	3.56	9.21	3.32	7.84	15.61	0.60	-0.30	11.37	2385.0	2986.0	0.540
	3.5	0.7402	1.21	3.71	39.60	2.69	39.35	4.40	0.69					1.026
450[c]	2.0	0.6503	0.84	4.65	0.34	3.32	0.51	11.09	0.18	-4.68	2.89	1331.0	23.5	6.018
	2.5	0.5566	1.46	5.70	0.60	3.99	0.63	3.46	0.11	-23.44	22.43	4478.0	43.1	25.150
							Dry runs							
22	2.5	0.6923	0.28	0.95	0.16	0.70	0.16	0.93	0.06	-0.11	0.34	75.0	5.6	0.361
	3.0	0.7240	0.38	0.34	3.33	0.21	3.28	6.26	1.15					0.135
80	2.0	0.6683	0.82	0.54	1.82	0.39	1.67	36.79	2.48					0.150
	2.5	0.6877	0.37	0.69	2.90	0.44	2.64	5.37	0.43	0.16	0.45	56.9	2.6	0.086
200	2.7	0.7444	0.85	0.39	2.48	0.43	2.35	9.82	0.72					-0.035
370	2.0	0.7043	0.53	0.34	1.00	0.34	0.82	96.18	6.54					0.000
	2.5	0.7372	0.28	0.74	2.98	0.64	2.57	3.37	0.21	-0.18	0.57	27.2	0.8	0.285
	3.0	0.7597	0.30	0.53	4.34	0.32	4.30	5.10	0.74					0.207
416	2.5	0.7191	0.45	0.59	3.95	0.65	3.11	3.96	0.55	-0.33	5.33	13.0	1.1	0.271
559	2.0	0.7116	1.05	1.63	1.86	1.40	2.14	2.00	0.26	-0.06	3.82	25.0	34.4	0.285
	2.5	0.7432	2.19	0.85	3.38	0.35	4.45	9.73	12.02	0.25	6.33	180.6	141.7	0.246
	3.0	0.7586	1.05	1.30	7.04	0.70	3.37	48.55	15.16	0.54	5.11	194.5	38.2	0.054
702	2.5	0.7664	1.12	1.32	12.40	0.99	9.14	7.66	1.53	-0.09	5.11	35.4	15.5	0.415
	3.0	0.7805	0.50	1.95	0.58	1.39	0.61	3.00	0.20	0.26	1.13	69.4	4.5	0.298
845	2.5	0.7673	1.77	1.67	13.23	1.38	12.74	9.03	0.97					0.289
	3.0	0.7855	0.42	1.43	7.72	0.89	7.26	8.88	0.92	0.53	0.78	100.9	2.6	0.009
600[d]	2.0	0.7229	0.87	3.11	0.81	1.99	0.99	7.60	0.27	1.58	1.57	152.9	3.3	-0.459
	2.5	0.7738	0.65	4.06	0.40	3.59	0.57	1.58	0.04	1.27	20.24	324.5	70.3	-0.805
	3.0	0.7960	1.29	4.73	0.80	3.54	0.85	4.45	0.16	1.61	1.23	222.3	6.1	-0.423
	3.5	0.8134	1.62	5.10	0.78	4.63	1.36	1.78	0.06	0.79	54.58	348.3	448.8	-0.319

For wet runs, pore pressure was 100 MPa. For dry runs, no pore fluid was used.

[a] Corresponding velocity steps were same as in Table 2.

[b] Pore pressure was 10 Mpa.

[c] Ten times slower slip rates were used.

[d] Data from experimental suite at constant normal stress of 400 MPa.

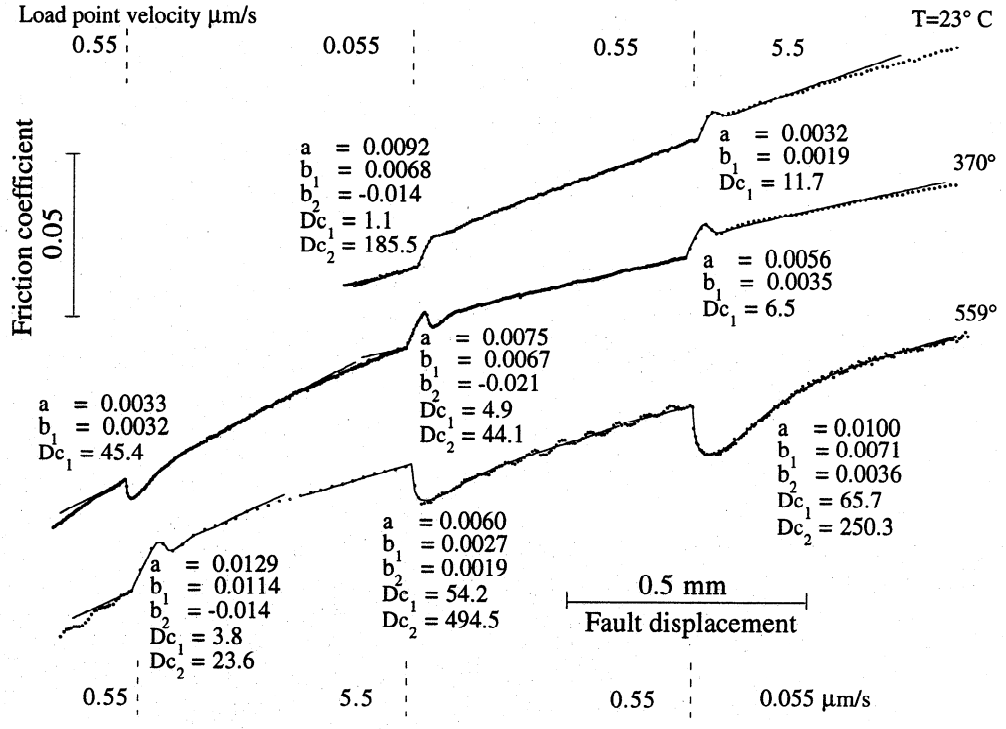

Figure 5. Representative data for dry granite gouge at three temperatures (dots). The response to each velocity step is fitted with the slip law, equations (2) and (3). (solid curves) by using the parameters listed by the step. (Small, periodic oscillations in friction, most clearly seen at 559° and $V = 0.55$ μm/s, were caused by fluctuations in temperature of <3°.) Velocities for top two traces are listed at top of figure; those for bottom trace are listed below. Parameter uncertainties are listed in Table 2.

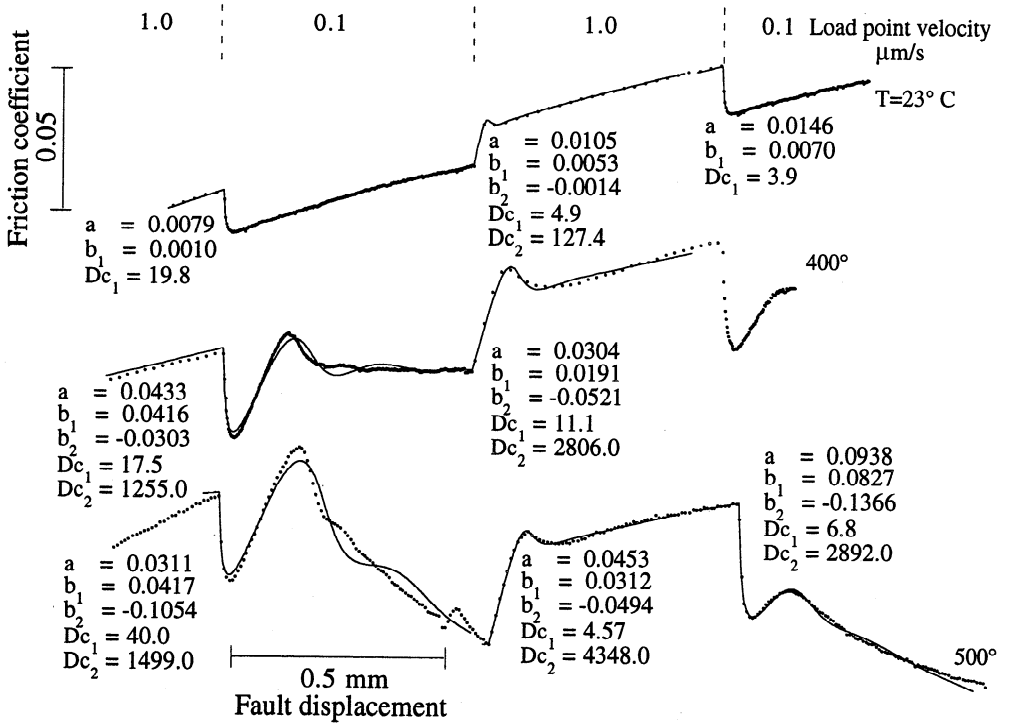

Figure 6. Representative data for wet granite gouge (dots). The response to each velocity step is fitted with the slip law (solid curves). For two of the steps at 23° a satisfactory fit was obtained by using one state variable. For the third velocity step at 400°, insufficient data are available to determine whether a second state variable is required to describe the behavior. Parameter uncertainties are listed in Table 2.

above 350° is fitted with a second state variable with longer characteristic displacement ($D_{c2} > 1000$ μm) and negative amplitude ($b_2 < 0$). Inversions using the slowness law (4) (not shown) yielded similar features.

Uncertainties in the parameter values derive principally from three sources. First, as we discussed above, the work-hardening trend C is determined by inspection of the data. The values of b_2 and D_{c2} are especially sensitive to the value of C. Second, in some cases the evolution of strength toward steady state is not complete after 0.5 mm, at which time the next step is imposed. This problem is most pronounced in wet runs at high temperature (Figure 2). Third, the compliance of the apparatus means that the velocity "steps" are not step-like. Gradual acceleration or deceleration toward the new slip rate results in a rounding of the transient peak and hampers accurate determination of parameters a, b_1, and D_{c1}. Covariance between a and b_1 is particularly acute when a is large and D_{c1} is small [*Reinen and Weeks*, 1993].

Figure 7 shows parameter values obtained by using the slip law, plotted against inverse absolute temperature. Scatter in the data likely reflects a combination of experimental reproducibility, changes in parameter values with increasing displacement, and uncertainty in the inversions from the several sources discussed earlier. Trends in the data, and the procedure by which we fit straight lines to the data (gray bands), are described in section 3 below. The choice of plotting against linear versus inverse temperature is largely arbitrary. Since both the data at hand and our understanding of the sliding process are insufficient to determine a correct representation, we follow the lead of *Chester and Higgs* [1992] who plotted a-b against T^{-1} following the form of their temperature-dependent constitutive law.

2.2. Multistep Fits

Nine experiments were analyzed in a second manner: The data from the entire rate-stepping portion of an experiment was inverted at once to obtain a single set of constitutive parameter values. We term these "multistep fits." Multistep fits were performed by using all three forms of the constitutive law, in order to compare the performance of the laws. Many, but not all, experiments lent themselves to this analysis; we rejected runs that displayed a non-linear trend and those for which steady state friction was not well defined in relation to the trend. (For example, in some runs, friction appeared to evolve toward different steady state values during sections at the same velocity, *e.g.*, the run at 845° in Figure 1).

These inversions require some modification to the procedure outlined above for individual steps. The data points are spaced

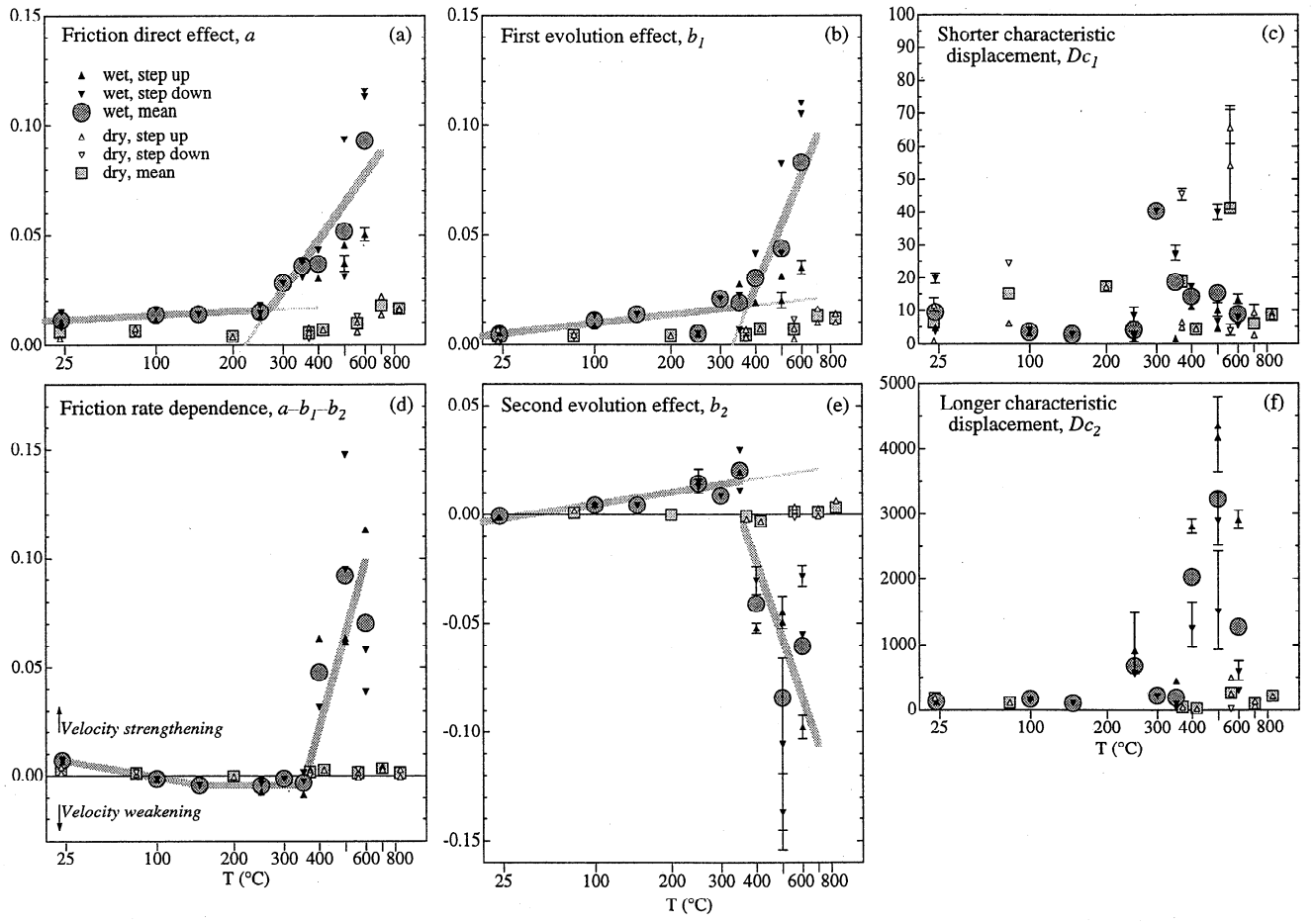

Figure 7. Constitutive parameters for dry and wet granite gouge versus temperature (data plotted versus $1/T$ in Kelvins, axis labeled in degrees Celsius). Wet data shown only for $P_p = 100$ MPa and steps between 1 and 0.1 μm/s. Small symbols are values obtained from modeling a single velocity step by using the slip law; see Table 2. Error bars (drawn where the error exceeds the symbol size) show the formal uncertainty for that parameter; other sources of uncertainty are discussed in the text. Larger symbols show the mean of the 1–4 values at each temperature. Grey lines show piece-wise linear regressions to the mean data values for wet gouge (circles). We fitted the mean values of parameters a, b_1, and b_2 in two segments and (independently) fitted the values for a-b_1-b_2 in three segments. The regression equations are listed in Table 5.

evenly in time, such that there are 10 times more points per displacement at the slow rates than at the fast rates. We weighted the fast portions 10 times more heavily such that the weighting per displacement was constant. We also experimented with more complicated weighting schemes, such as weighting more heavily points immediately after each velocity step; however, the fits were not markedly improved.

Unlike the single-step fits described above, multistep fits assume steady state conditions only prior to the first velocity step. Steady state may or may not be reached before subsequent steps, depending on the values of the constitutive parameters, especially b_2 and D_{c2}. (State may in fact be evolving even at the time of the first step, but since we have no independent means to measure state, we make the simplifying assumption that it is not.) This approach is appealing because it is clear that steady state was not reached between velocity steps in some experiments, especially wet runs at the highest temperatures (Figure 2). We took care to ensure that each of the three inversions for a given run began with the same initial conditions.

Figure 8 shows data from five experiments, one dry and four wet, along with multistep fits obtained by using the three constitutive formulations. Table 4 lists the best-fit parameter values and their uncertainties. In general, the simulations do not fit the data as perfectly as those shown earlier, because the best-fit parameter values are "compromise" values that minimize the misfit for the entire data set. At 23°C the three fits nearly overlie one another and fit the data well, and the parameter values, except for b_2, are identical within the level of uncertainty. Likewise at 250° and 450° the three fits are quite similar, and each captures the general form of the transient friction response, although the match to the data is not perfect. At 250° a single state variable is required (in contrast to the fits for individual steps), and at 23° the value of b_2 is small and the second state variable improves the fit only marginally. The situation is somewhat different for the two runs at 600°. For dry granite (top trace) all three constitutive laws match the downward steps well and match the upward steps poorly. The slowness law (4) is asymmetric with respect to the sense of the velocity step. This feature is evident in the simulations: The evolution of friction following upward steps is longer than that following downward steps, with a best-fit value of D_{c2} (96 μm) about twice that for the other two fits. The data are also asymmetric but in the opposite sense: They show a more rapid evolution to steady state following upward steps. Thus the slowness law is the least adequate of the three to model this experiment. For wet granite at 600° (bottom trace), none of the laws matches all details of the data. However, given the complex behavior displayed at these conditions, it is perhaps encouraging that the fits capture the general form and magnitude of the transient response.

It is interesting to note that the inversions at 450° and 600° (Figure 8) did not require a work-softening trend. The experimental data suggest to the eye that the response to velocity steps is superimposed on a gradual weakening. However, satisfactory fits are obtained with the trend parameter C set to zero. The visual appearance of a downward trend results because friction does not reach steady state between velocity steps. Both of these experiments showed an initial peak friction followed by relaxation to a nearly steady strength at the point of the first velocity step, in agreement with the choice of $C = 0$.

The values for wet granite determined in this manner are plotted along with those determined from single steps in Figure 9. In all but a few instances the parameter values for the three methods cluster closely and fall within the range of values determined from single steps. For the experiment at 600°C the inversion using the quadratic law found low values for both a and b_1. Recall

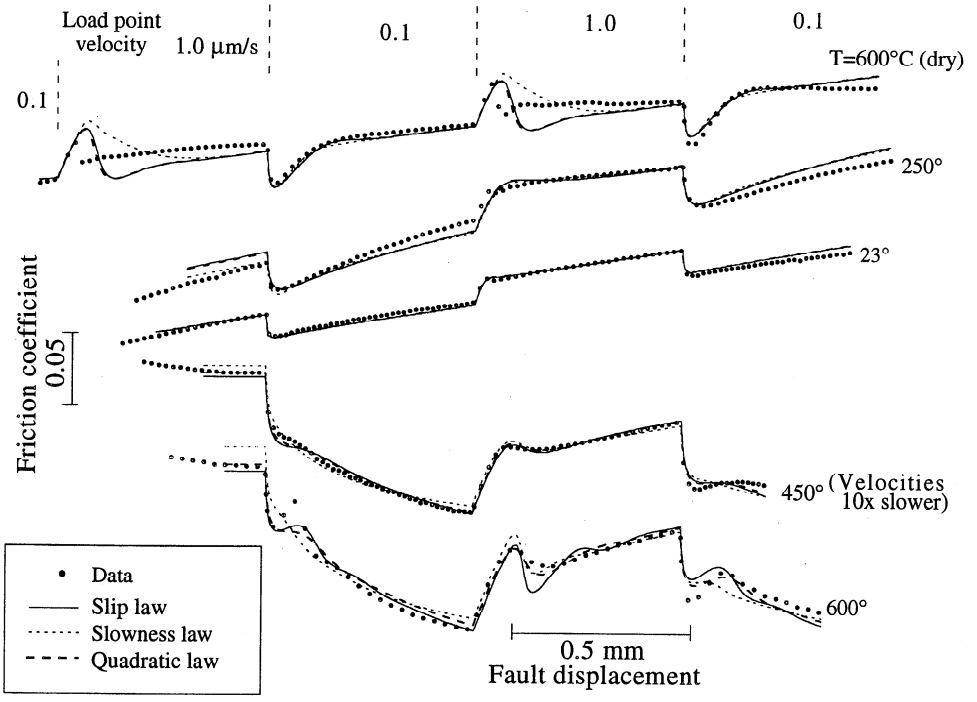

Figure 8. Data (dots) for several contiguous steps in selected experiments, fitted with the three forms of the constitutive law (solid and dashed lines). For each inversion a single linear trend was chosen (shown by the slope of the simulations to the left of the first velocity step), and a single set of parameters was determined. See text for details on the fitting procedure. Table 4 lists the best fit parameter values. Data have been shifted vertically for clarity. Velocities for the run at 450°C were 0.1 and 0.01 μm/s.

Table 4. Parameter Values Determined by Fitting Multiple Velocity Steps

T, °C	Law[a]	μ	μ s.d. x10^{-4}	a x10^{-2}	a s.d. x10^{-4}	b_1 x10^{-2}	b_1 s.d. x10^{-4}	D_{c1}, µm	D_{c1} s.d.	b_1 x10^{-2}	b_2 s.d., x10^{-4}	D_{c2}, µm	D_{c2} s.d.	$a-b_1-b_2$ x10^{-2}
							Wet runs							
23, 3 steps														
	slip	0.6509	2.16	0.81	14.53	0.10	13.32	10.56	57.69	0.06	1.69	167.7	137.8	0.655
	slow.	0.6512	2.29	0.80	14.47	0.10	14.05	9.79	50.48	0.02	1.66	255.9	926.7	0.681
	quad.	0.6509	2.30	0.82	19.08	0.09	17.63	9.10	120.90	0.08	1.97	199.7	193.1	0.651
100, 2 steps														
	slip	0.6576	1.50	0.99	16.71	0.72	16.05	4.44	1.38	0.36	1.15	149.8	11.1	-0.083
	slow.	0.6561	1.97	1.28	1.06	1.00	1.12	2.31	0.31	0.38	1.99	118.5	11.6	-0.099
	quad.	0.6577	1.58	1.13	0.84	0.79	0.90	3.10	0.44	0.43	1.30	179.0	15.8	-0.089
250, 3 steps														
	slip	0.6942	6.67	1.40	4.04	0.88	3.46	255.40	25.64					0.520
	slow.	0.6876	6.76	1.34	3.66	1.02	3.23	273.80	19.11					0.324
	quad.	0.6933	6.95	1.41	3.98	0.98	3.92	358.10	38.00					0.430
350, 3 steps														
	slip	0.6841	4.36	1.61	7.12	0.69	10.13	55.21	17.45	1.52	11.57	260.2	22.0	-0.598
	slow.	0.6722	3.99	1.79	19.18	0.61	18.08	14.42	7.47	2.00	3.39	223.3	6.1	-0.829
	quad.	0.6818	4.37	1.56	6.72	0.49	10.41	58.45	31.54	1.91	12.45	370.4	26.1	-0.835
600, 3 steps														
	slip	0.6331	7.86	11.90	1.56	11.07	1.55	5.22	0.14	-5.45	6.16	468.4	7.7	6.275
	slow.	0.6500	10.19	12.09	2.87	10.81	2.91	3.49	0.28	-4.66	7.11	523.0	16.0	5.941
	quad.	0.6377	8.10	4.97	38.66	4.18	35.78	21.01	2.56	-5.86	7.22	662.9	16.0	6.650
600[b], 3 steps														
	slip	0.7337	3.48	3.86	11.56	2.75	10.50	32.13	1.69	1.95	6.73	1335.0	113.0	-0.842
	slow.	0.7257	3.90	3.35	10.56	2.15	9.56	35.25	2.41	1.52	2.91	818.7	41.3	-0.322
	quad.	0.7319	3.25	3.89	10.79	2.76	9.82	31.62	1.68	1.91	3.69	1739.0	106.4	-0.777
450[c], 3 steps														
	slip	0.6484	3.02	3.07	10.36	1.73	8.97	32.55	2.61	-4.05	2.76	527.8	6.3	5.389
	slow.	0.6561	3.67	2.68	19.77	1.23	18.79	20.68	4.47	-3.29	2.97	515.4	8.7	4.738
	quad.	0.6512	2.27	3.11	6.50	1.94	5.27	42.17	2.43	-4.41	2.68	664.8	7.4	5.578
							Dry runs							
80, 3 steps														
	slip	0.6685	2.03	0.33	1.62	0.39	1.41	203.50	19.45					-0.061
	slow.	0.6676	2.79	0.32	1.42	0.39	1.50	229.90	20.51					-0.068
	quad.	0.6685	2.30	0.35	1.84	0.42	1.73	276.40	32.48					-0.075
600[c], 4 steps														
	slip	0.7747	1.50	3.45	4.97	1.65	5.07	1.14	2.28	1.89	10.08	45.7	2.3	-0.088
	slow.	0.7744	1.63	3.84	2.65	2.44	2.82	3.38	0.63	1.50	4.94	95.9	4.6	-0.102
	quad.	0.7747	1.51	3.72	4.16	1.84	4.20	0.37	4.68	1.96	8.59	52.7	2.8	-0.082

In all cases the first velocity step of the modelled sequence occurred at 2.0 mm displacement; the total number of steps modeled is listed after the temperature. For wet runs, pore pressure was 100MPa. For dry runs, no pore fluid was used.

[a] Constitutive law "slip" is the slip law, "slow." is the slowness law, "quad." is the quadratic law.

[b] Pore pressure was 10MPa.

[c] Ten times lower slip velocities were used.

[d] Data from experimental suite at constant normal stress of 400 MPa.

that these two parameters are highly correlative, so a substantial increase in both a and b_1, at fixed a-b_1, would do little to degrade the goodness of fit.

One important point regards our interpretation of the inversion results for the experiment at 250°. When each of this run's three steps was analyzed separately, it was fitted with two state variables. However, the run as a whole was fitted with only a single state variable. We have examined the best-fit simulations and the parameter values, and find that the dominant evolution, in other words the evolution fit by the single state variable in the latter case, is the evolution fit by b_2 and D_{c2} in the former case. Therefore we plot the values for b and D_c on the graphs for b_2 and D_{c2} (Figure 9b,e) rather than on the plots for b_1 and D_{c1}. Note that these values show good agreement with values at adjacent temperatures.

2.3. Effects of Slip Rate and Fluid Pressure

Most of the sliding experiments were performed at a fixed set of conditions and slip rates. The principal comparisons that can be made are between dry and wet experiments at similar temperatures. However, a few wet experiments were performed at tenfold slower rates, and runs were performed at lower P_p (Tables 2 and 3), allowing some additional comparisons to be made. Figure 10a shows friction-displacement curves for two pairs of runs on wet gouge. Within each pair the traces appear similar in strength and in response to steps in velocity. In the upper pair, data for a standard run at 300° are nearly overlain by data for a slow run at 250°. Both traces include a small stick-slip event following an upward step in velocity at 2.5 mm. In the lower pair, data for a standard run at 600° are nearly overlain by data for a slow run at 450°, although some details of the transient response are not well matched in this case. These runs illustrate the degree to which temperature and slip rate may compensate one another at hydrothermal conditions [see also *Chester*, 1995]. A portion of each run is replotted in Figure 10b along with a model fit using the Ruina formulation. Constitutive parameters for the fits at 450° and 600° are similar in value. The difference between them is less than the scatter for repeated steps at the same temperature (cf. Figure 7). Parameters for the fits at 250° and 300° agree less well.

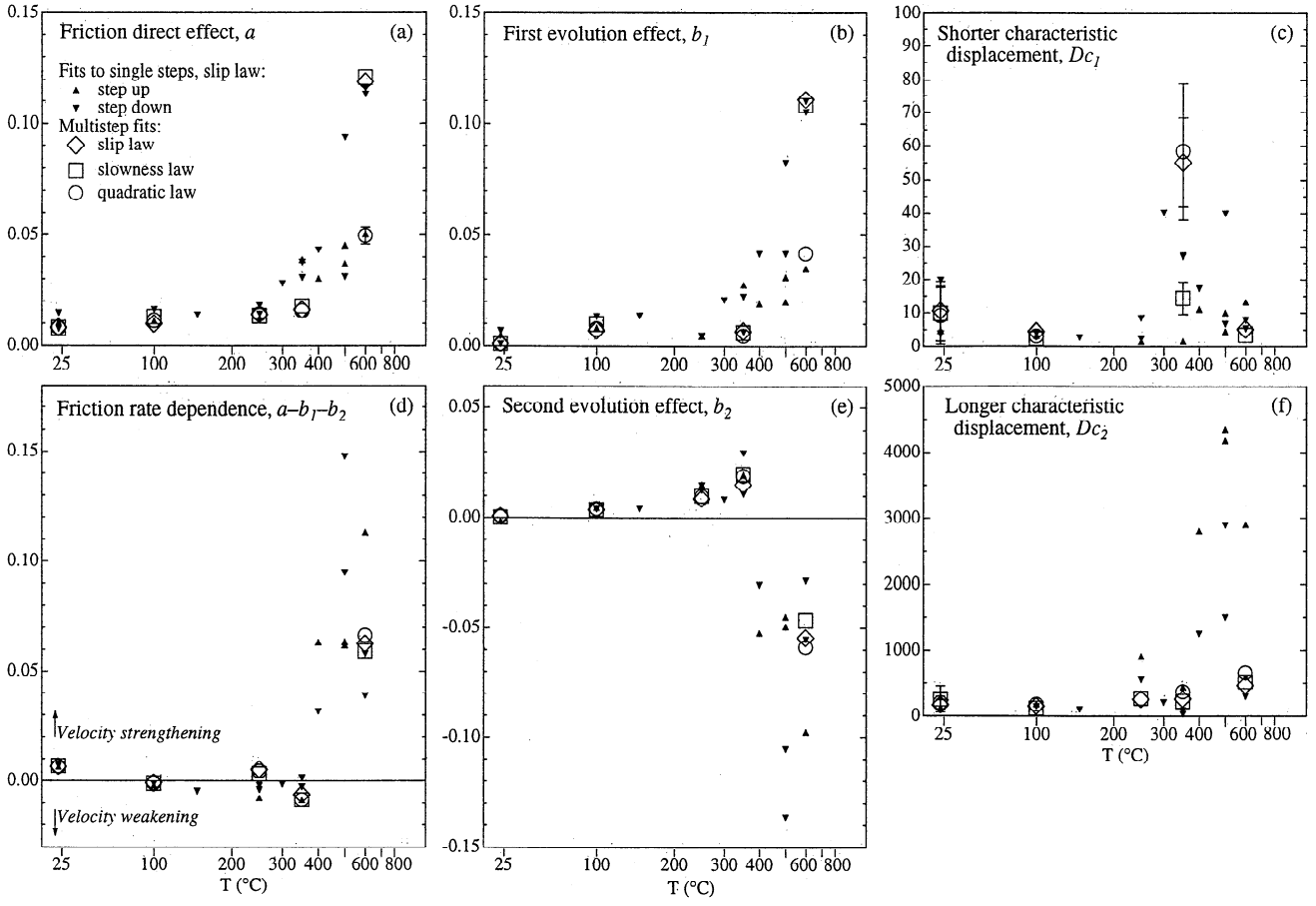

Figure 9. Parameter values for wet granite gouge determined by inversion of individual velocity steps (solid triangles), values from Figure 7 and Table 2, and values determined by multistep fits, i.e., inversion of several velocity steps in a run (open symbols). Error bars shown for multistep values only, where they exceed the symbol size. See text for additional comments.

In Figure 11a we compare three experiments with different pore pressures. All three runs were done at 600°C and at the same constant effective normal stress of 400 MPa. The sample marked "dried" was vacuum dried during heating and while resting at 600° for ~1 hour, then was vented to the atmosphere during deformation. The dry coefficient of friction is about 0.8, and velocity steps cause a strength transient but almost no change in steady state friction level. With the addition of 10 MPa P_p the friction at the higher slip rate is nearly unchanged, but the friction at the lower slip rate is depressed by 0.015 to 0.025 in comparison with the dried run. With 100 MPa P_p the friction is depressed at both rates, though much more so at the slower rate, and velocity steps are followed by prolonged evolutions of strength containing multiple reversals. Figure 11b shows best-fit simulations using the slip law. Not surprisingly, the most striking trend is in the value of parameter b_2: The steps for dry granite and 10 MPa P_p are fitted with a modest, positive value of b_2 (0.0026 to 0.0133), while the pronounced evolution when P_p = 100 MPa is fitted with a large, negative value (–0.0284 to –0.0976). Although the size of the direct peak increases with increasing P_p (compare the upward steps), the values of a do not reflect this trend. Similarly, values for b_1 and D_{c1} show no obvious trends, and D_{c2} shows wide scatter.

3. Discussion

3.1. Trends in Parameter Values

The parameter values for dry granite are fairly uniform over the entire range of temperatures tested, while those for wet granite show distinct trends (Figure 7). Parameter a for wet granite shows a small, positive dependence on temperature to 250° but a much stronger dependence at higher temperatures (Figure 7a). Parameter b_1, associated with the first state variable, which evolves more quickly with displacement, shows a similar pattern (Figure 7b), although values at 250° are small in relation to those at 150° and 300°. The characteristic displacement D_{c1} for both wet and dry granite shows scatter but is less than 70 μm at all temperatures (Figure 7c). Parameter b_2 is shown only where a second state variable was found necessary (Figure 7e). Values of b_2 for dry granite are small ($|b_2| \leq 0.0063$) and sensitive to the exact value of the trend chosen. In fact, given the subjectivity in the detrending process, we cannot say with confidence that values of b_2 for dry granite differ from zero; visually adequate fits to nearly all steps for dry granite can be obtained by using one state variable only. Values of b_2 for wet granite show a distinct pattern: Below 400°, b_2 increases with temperature, and $D_{c2} < 1000$ μm.

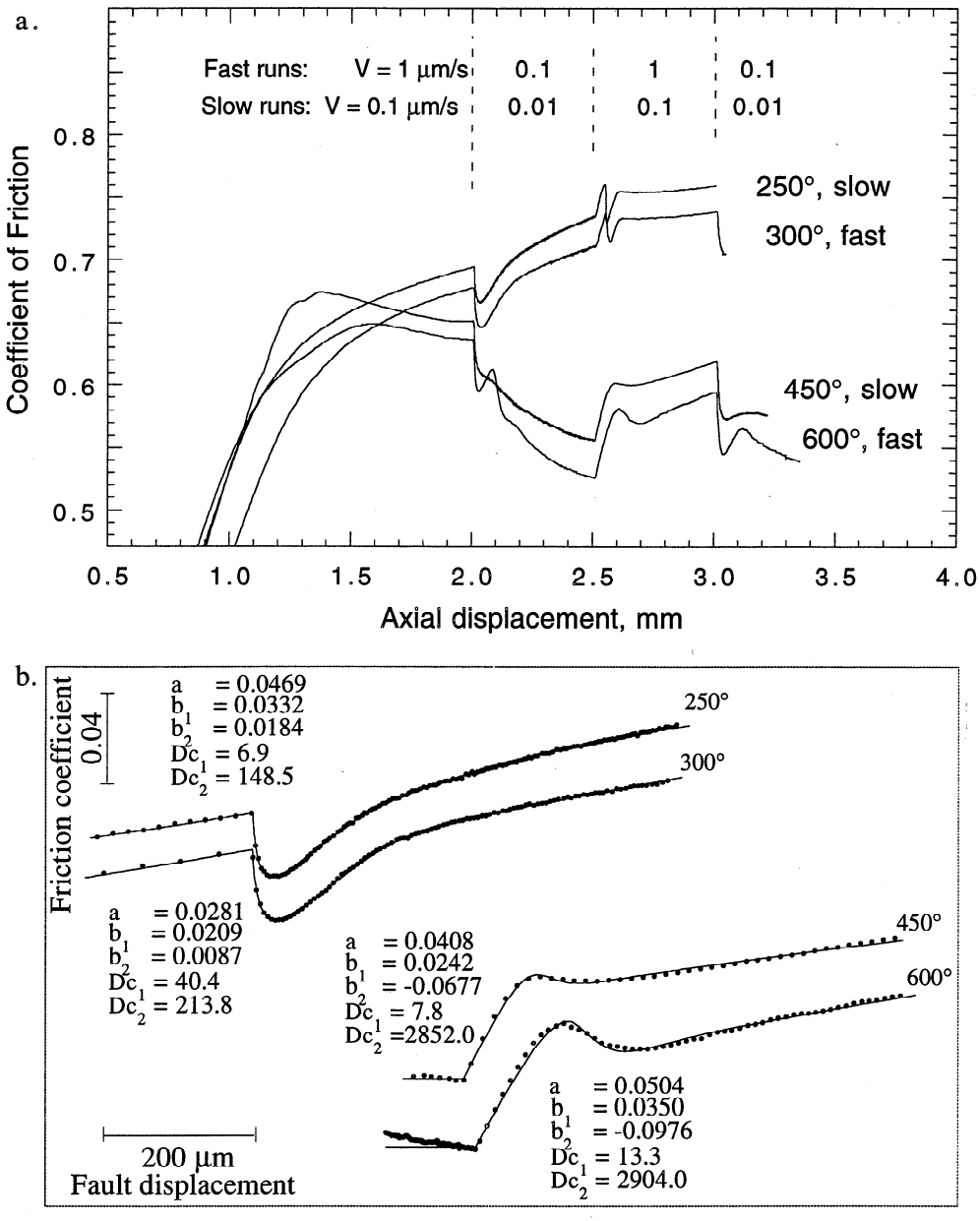

Figure 10. (a) Friction-displacement curves for two pairs of runs on wet granite gouge with P_p = 100 MPa illustrating the degree to which temperature and slip rate may be exchanged at hydrothermal conditions. (b) Data for one velocity step from each of the four runs (dots) and bestfit simulations using the Ruina form of the constitutive law (curves). The value of the trend parameter C is the same within each pair.

At 400° and above, b_2 has large, negative values and is associated with values of D_{c2} of 1000 to 5000 μm (Figure 7f). Recall that a negative value of b_2 means that friction evolves in the same sense as the direct effect. Examined together, Figures 2, 6, and 7 show that for wet granite at high temperatures the first state variable fits the short-term evolution of strength following the direct effect peak, while the second state variable fits the protracted evolution of strength that follows. The sum of b_1 and b_2 is slightly negative at these conditions, meaning that the net velocity dependence a-b_1-b_2 is positive and surpasses the direct dependence a. This feature is suggested by the friction-displacement records at 500° and 600° in Figure 2.

Dry granite shows neutral to slightly positive velocity dependence at all temperatures tested (Figure 7d). The single value at 200° is negative (–0.0003), while average values at all other temperatures are positive. A positive dependence on temperature is evident above 400°. Wet granite shows more pronounced trends: From 23° to 150°, a-b_1-b_2 decreases from positive to negative, because b_1 and b_2 increase with temperature more than does a. Values from 150° to 350° mostly fall in the range –0.01 to zero. From 400° to 600° a-b_1-b_2 is strongly positive because of the large and negative values of b_2.

Examination of Figures 7a and 7b shows that for wet granite, larger values of a and b_1 result from downward velocity steps rather than from upward steps for almost all runs analyzed. The effect is also seen in the parameters found by using the slowness law (4) (Table 3). It is not clear whether this effect is a feature of the data or results from bias in the modeling technique. It is possible that the bias results from the pore-pressure transients described earlier: A step from 0.1 to 1 μm/s causes the gouge to

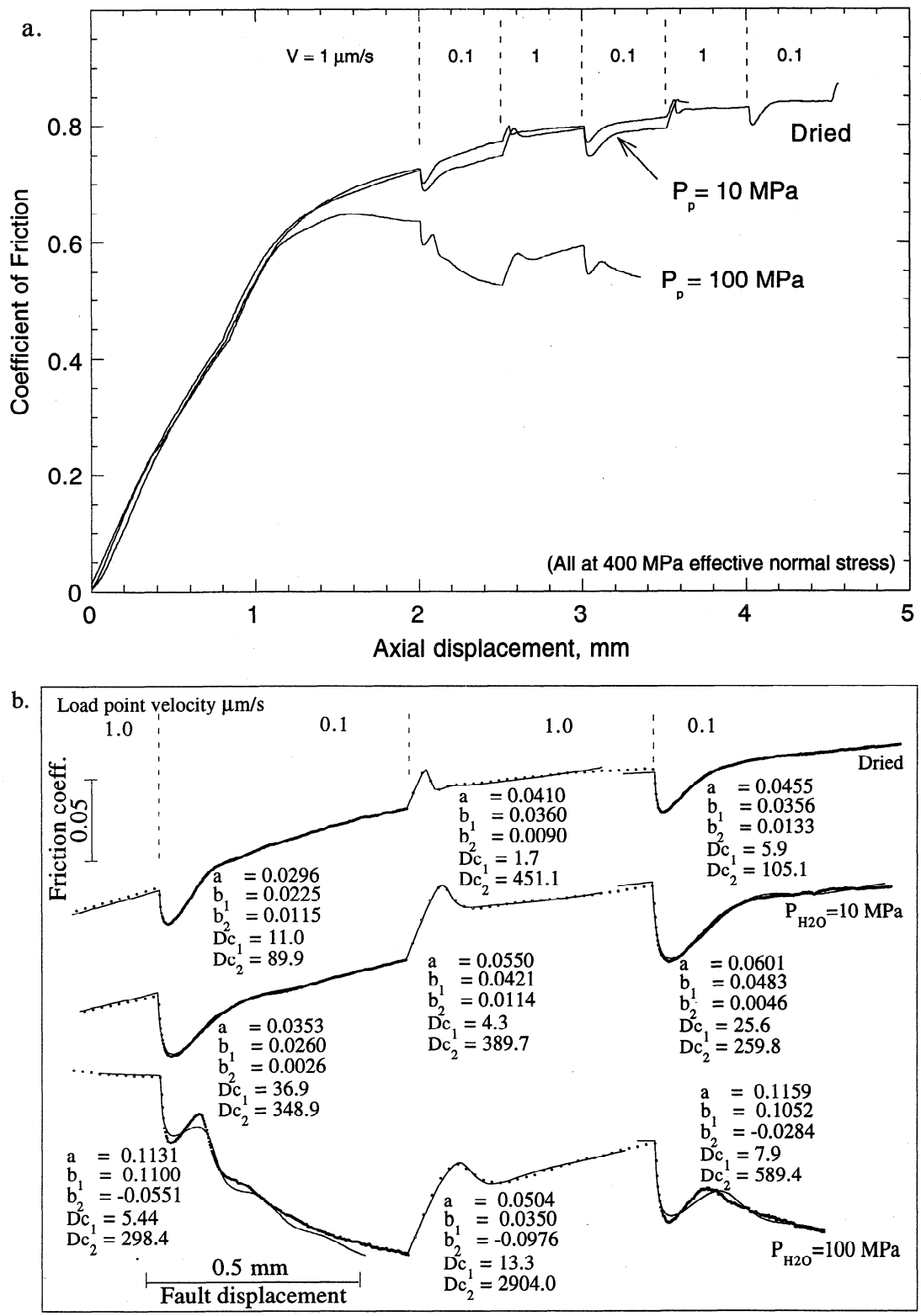

Figure 11. (a) Friction-displacement curves for granite gouge slid at 600°C, effective normal stress of 100 MPa, and pore pressures of 0, 10, and 100 MPa. Elevated P_p causes weakening even at constant effective stress. Weakening is more pronounced at the lower slip rate. (b) Data (dots) and simulations (curves) for the same three experiments. Both the velocity dependence of friction and the transient response to velocity steps are affected by changing P_p. Velocity steps at P_p = 100 MPa are followed by a long-term evolution of strength in the same sense as the direct response (initial peak). This long-term evolution can be modeled by a second state variable with b_2 negative.

dilate [*Marone et al.*, 1990; *Lockner and Byerlee*, 1994; *Beeler et al.*, 1996; *Segall and Rice*, 1995]. Rapid dilation of the gouge may result in a temporary drop in fluid pressure, thereby limiting the acceleration of slip and attenuating the direct effect peak. (A similar argument was made by *Higgs* [1981].) The inversion method does not account for such transient effects, so they may be reflected in reduced values of the parameters a and b_1. Two observations support this hypothesis: First, the effect is greatest at 400°–600°C, temperatures at which the permeability of the granite may be lowered rapidly as a result of solution transport or the formation of clays [*Blanpied et al.*, 1992; *Moore et al.*, 1994; *Olsen et al.*, 1998]. Second, the parameter values for dry granite show no systematic bias. If pore pressure transients do occur, then the downward velocity steps give a truer measure of the constitutive parameters in wet runs. On the other hand, recall that the values of parameters a and b_1 are highly correlated and are poorly determined in relation to their difference a-b_1, because of the compliance of the loading system (Figure 5), so systematic errors arising from the inversion technique cannot be ruled out.

Trends evident in Figure 7 and discussed above are similar to those described by *Lockner et al.* [1986] and *Blanpied et al.* [1991, 1995]. Neither group modeled velocity steps to quantify the individual parameter values as was done here. However, both calculated the net velocity dependence (which does not require modeling) from measurements of $\partial\mu_{SS}$ made by hand off the friction-displacement records. Values of $\partial\mu_{SS}/\partial \ln V$ ($= a$-b_1-b_2) shown in Figure 7d agree well with their results, even though different researchers chose the detrending slopes. For example, *Blanpied et al.* [1991] plotted a range of values of $\partial\mu_{SS}/\partial \ln V$ from 0.029 to 0.044 for wet gouge at 600°, which agrees well with the current range (0.029 to 0.054). *Lockner et al.* [1986] measured a rough value for the characteristic evolution displacement directly from the friction-displacement records. Their values for dry gouge generally increase with temperature, with considerable scatter; most of their values were in the range 0 to 200 μm (their Figure 6), in agreement with the present data for D_{c1} and D_{c2} (Figures 7c and 7f, open triangles).

Values of a and a-b_1-b_2 for granite gouge agree well with results for ultrafine quartz gouge reported by *Chester and Higgs* [1992] (Figure 12). Experiments were conducted at temperatures of 23°, 300°, 450°, and 600°C, effective pressure of 150 MPa, and P_p of either 0 (dry) or 100 MPa (wet) [*Higgs*, 1981]. *Chester and Higgs* [1992] fitted the response to slide-hold-slide (relaxation and reload) tests, using the slip law with one state variable. The value of D_c was not well constrained. Dry quartz shows velocity strengthening at 23° and velocity weakening at 300° and 450°; values for a are small and agree well with those for granite. Wet quartz shows velocity neutral response at 23°, velocity weakening at 300°, and substantial velocity strengthening at 600°. (The 600° data were modeled adequately with $b = 0$; thus a-$b = a = 0.03$.) Values of a and a-b_1-b_2 at 600° are lower for quartz than for granite; however, in both cases there is a substantial rise in value in the hydrothermal regime.

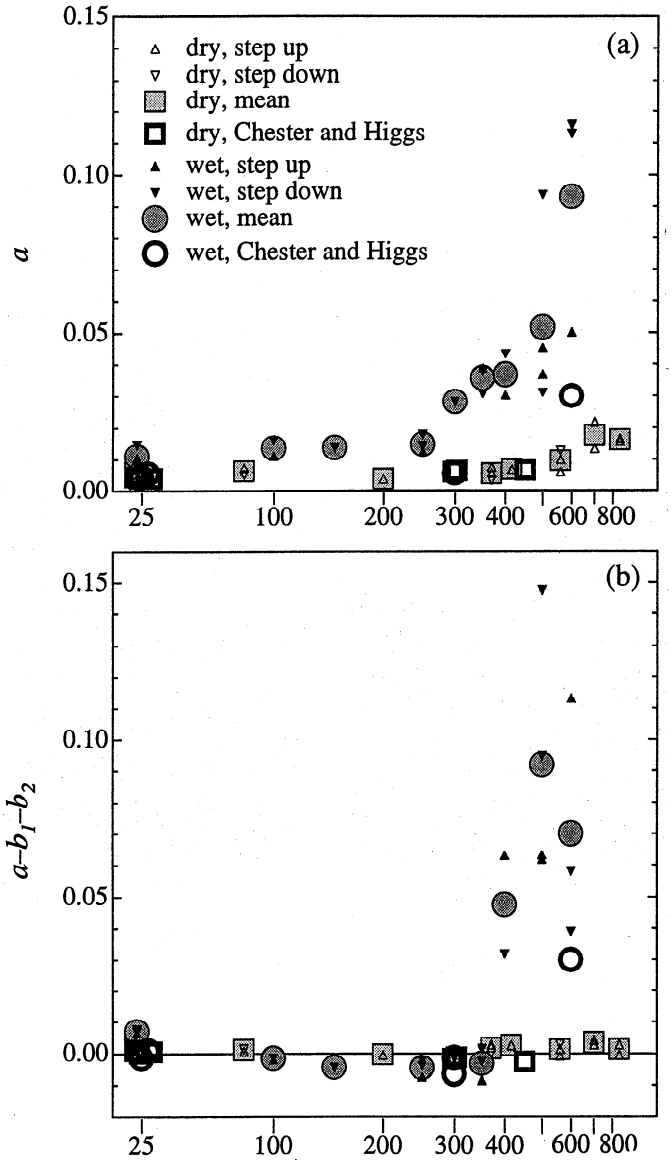

Figure 12. Values of parameter a and velocity dependence a-b_1-b_2 for granite (this study) and for quartz gouge [*Chester and Higgs*, 1992]. Values for granite are the same as those in Figures 7a and 7d. Large, shaded symbols are means for values at a given temperature. Values for quartz were determined by modeling slide-hold-slide (stress relaxation and reload) tests. Conditions for quartz experiments: 150 MPa effective pressure and 0 (dry) or 100 MPa (wet) P_p.

3.2. Quantifying Trends

One main purpose of our study is to quantify trends in constitutive parameter values as a function of temperature. We do this to help understand the physical basis for rock friction behavior and to provide a basis for the use of the experimental friction results in earth models.

The decision to plot parameter values against inverse temperature (Figure 7) rather than linear temperature was somewhat arbitrary. Our goal was to highlight trends in the data; given the limited range of temperatures tested, and the amount of scatter, equally clear trends appear plotted both ways. A temperature-dependent friction constitutive law has not yet been derived from first principles [*Sleep*, 1995], and the mathematical relationship between the constitutive parameters and temperature remains unclear. As we discussed in the introduction, our expectation is that the values of constitutive parameters reflect the rate of associated deformation micromechanisms active in the sliding process. The rates of those thermally activated mechanisms vary with temperature through an Arrhenius relation, and it is reasonable to speculate that the value of a constitutive parameter varies linearly with inverse temperature within the conditions of dominance of a given deformation mechanism. Similar, though mathematically

distinct, reasoning was earlier employed by *Chester* [1988, 1994] and *Chester and Higgs* [1992], who developed a temperature-dependent constitutive law by adding Arrhenius-like terms to Ruina's equations for friction (2) and the evolution of state (3), using a single state variable.

We have highlighted trends in Figure 7 by piecewise linear regression to the mean values for wet gouge. Thin gray lines show the linear regressions; thicker lines represent the combined data set. Regressions were performed to quantify trends and slope breaks in the hope that this method can facilitate linking parameter values to deformation micromechanisms, and also to provide a convenient representation of parameter values for use in numerical fault models. Table 5 shows which values were included for each determination. The combined representation for parameter b_2 was purposefully left discontinuous, for reasons explained later.

We chose to use two line segments to represent the data for a, b_1 and b_2, for the following reasons: Examination of the plots makes it clear that a single line is inadequate to represent the variation of a, b_1 or b_2 with inverse temperature. Rather, abrupt changes in trend coincide with abrupt changes in sliding behavior of wet gouge. For example, the magnitude of the direct effect peak for wet gouge is nearly constant up to 200°C and increases rapidly with higher temperature (Figure 2); this feature is reflected in the rapid increase in a above 200° (Figure 7a). As a second example, velocity steps at ≥400° are followed by a prolonged evolution in the same sense as the velocity step, a feature absent at lower temperatures (Figure 2); this is reflected in large, negative values of b_2 at the higher temperatures only (Figure 7e). Two straight lines on each subplot are adequate to represent these features of the data set. Additional line segments could be used to more closely match trends in the data (e.g., for b_1 between 150° and 350°C); however, additional line segments would be defined by data at only two or three temperatures, which we feel to be insufficient to define trends with confidence. Although higher-order fitting functions could be applied, we have neither the theoretical justification nor the data to provide guidance.

We have not fitted lines to values of D_{c1} and D_{c2}, although there are systematics evident in those values as discussed earlier. The complex distribution (scatter?) of those values, especially at higher temperatures, makes it difficult to represent trends with a simple function. We have also not fitted lines to the parameter values for dry granite. Trends are more subtle for the dry values, though some features are evident. *Lockner et al.* [1986] noted that the direct response to slip rate steps is larger at the highest temperatures. For example, both a and b_1 are nearly constant at ≥400°C and rise at higher temperatures (Figures 7a and 7b). *Lockner et al.* [1986] estimated a characteristic evolution displacement directly from friction-displacement curves and noted an increase in evolution displacement with temperature; this trend is not so clearly expressed in our values for D_{c1} and D_{c2} (Figures 7c and 7f).

The line segments drawn to represent a-b_1-b_2 (Figure 7d, Table 5) were determined independent of those drawn for a, b_1 and b_2. It would seem logical that subtracting the lines for b_1 and b_2 from the line for a would yield an adequate representation for values of a-b_1-b_2. However, this supposition is not true because of our decision to restrict the number of line segments for each parameter to two. In particular, the value of b_1 at 250°C is poorly represented by the bilinear fit; thus a simple subtraction yields a value of a-b_1-b_2 of –0.0115, much lower than the mean value of –0.0044 at that temperature. The sign and magnitude of velocity dependence are often linked in the literature to sliding stability and earthquake hypocentral depths [e.g., *Tse and Rice*, 1986; *Blanpied et al.*, 1991], so an accurate representation is important. Also, a simple subtraction would yield a fit to a-b_1-b_2 composed of five segments, whereas Figure 7d suggests that three segments are adequate to represent major trends. For these reasons we calculated the three line segments in Figure 7d directly from the mean values of a-b_1-b_2 (Table 5).

3.3. Links to Deformation Mechanisms

We loosely define a "transition temperature" T_T as the temperature of intersection of two linear segments on a plot of parameter value versus inverse temperature. For wet granite the boundary between the two regimes is conspicuous, allowing us to define the straight-line fits in Figures 7a, 7b, and 7e. Values for

Table 5. Linear Representations of Mean Parameter Values for Wet Gouge (gray lines in Figure 7)

Parameter	T Range, °C	Regression Line	Data Used, °C [a]	D_c, μm [b]
		Constitutive parameters (Figures 7a, 7b, and 7e)		
a	T < 270	0.02127 – 3.00 / T(K)	23 to 150	
	T ≥ 270	0.17838 – 88.14 / T(K)	250 to 600	
b_1	T < 375	0.02795 – 6.87 / T(K)	23 to 350	2 – 10 μm
	T ≥ 375	0.25090 – 151.62 / T(K)	400 to 600	5 – 50 μm
b_2	T < 350	0.03089 – 9.79 / T(K)	23 to 350	100 – 200 μm
	T ≥ 350	–0.29301 + 182.59 / T(K)	400 to 600 [c]	1000 – 2000 μm
		Steady state rate dependence (Figure 7b)		
a –b_1–b_2 [d]	T < 150	–0.03061 + 11.14 / T(K)	23° and 150 [e]	
	150 ≤ T < 350	–0.00428	value at 150	
	T ≥ 350	0.3550 – 223.91 / T(K)	350° to 600 [f]	

[a] Range of mean values used in the linear regression, except where noted.
[b] Corresponding values of D_{c1} and D_{c2}. Most, but not all values fall in the ranges listed (see Figure 9).
[c] Line forced to pass through zero at 350°C. The representation for b_2 is discontinuous at that temperature.
[d] Representation of quantity a –b_1–b_2 is not equal to the sum of the representations of the three parameters above (see text).
[e] Straight line through mean values at 23° and 150°C.
[f] Regression through values for individual steps; regression forced to -0.00428 at 350°C.

T_T are 270°C for a, 375°C for b_1, and 350°C for b_2. *Blanpied et al.* [1995] discussed T_T for wet granite in more general terms and argued that T_T is depressed by a few tens of degrees per decade decrease in slip rate. They referred to a "hydrothermal regime," accessible at elevated T, elevated P_p, and low slip rates and characterized by high-amplitude transient response, extended approach to steady state, and stable sliding. In the context of rate- and state-dependent friction laws our inversion results suggest that this hydrothermal regime is characterized by increased values of a and b_1, large and negative values of b_2, and large values of D_{c2}.

Chester's [1994, 1995] temperature-dependent friction law assumes that the values of the constitutive parameters are constant within each regime, with the boundary between regimes marking a change in all parameters. Similar reasoning was used by *Reinen et al.* [1992] in modeling the strength of room temperature serpentinite gouge. At high sliding rates the gouge displayed the usual velocity and slip history dependencies, and the response to velocity steps could be modeled by using the slip law with one state variable. At low rates the gouge displayed a strong, viscous-like velocity dependence and no history dependence (i.e., large a and $b = 0$), behavior that Reinen et al. associated with dislocation glide. Presumably, the boundary between these two sliding regimes is a function of both velocity and temperature. Our method, in contrast, allows T_T to differ for each parameter. This is a reflection of our assumptions: (1) that each parameter may be associated with a particular deformation mechanism and (2) that T_T marks a change from one deformation mechanism to another (or a change of rate-limiting step). Experimental data do not currently exist with which to test such subtle distinctions.

Blanpied et al. [1992] discribe the appearance of an unidentified phyllosilicate mineral found on the sliding surface of wet samples slid at 500° to 600°C and at low slip rates. Small amounts of this mineral were found in topographic depressions in the localized sliding surface at the boundary of the gouge layer and may represent precipitation of biotite or clays following dissolution of feldspars. *Blanpied et al.* [1995] present largely circumstantial evidence that the water-aided mechanism is promoted by decreased particle size in the gouge, suggesting that the mechanism is rate limited by diffusion or depends on surface area.

Stronger evidence for the role of water comes from comparison with *Higgs*'s [1981] observations of quartz powder. Higgs noted a clear division of quartz behavior into two regimes similar to those discussed above for granite: Tests on cool and/or dry quartz gouge showed high strength and little loss of strength during stress relaxations to low strain rates. In contrast, tests at hot and wet (hydrothermal) conditions showed a pronounced loss of strength during relaxations. Furthermore, microstructural observations on the quartz gouges deformed at hydrothermal conditions revealed clear evidence that solution-precipitation creep accompanied cataclastic flow [*Chester and Higgs*, 1992]. *Fredrich and Evans* [1992] and *Karner et al.* [1997] have demonstrated as well that quartz powders can rapidly densify and lithify at hydrothermal conditions. Determinations of a and a-b for quartz (Figure 12) were made at temperatures too widely spaced for an accurate determination of T_T, except to say that it lies between 300° and 600°C. *Chester and Higgs* [1992] and *Chester* [1995] have argued that the activation of solution-transport deformation defines a separate deformation mechanism field for frictional slip. On the basis of microstructural observations for quartz and the correspondence in mechanical behavior between the quartz and granite gouges, we tentatively identify solution-precipitation creep as responsible for the decreased strength and increased rate dependence observed in the hydrothermal granite tests.

A negative value of b_2 necessitates an interpretation different than the usual one given to friction history dependence. The interpretation of *Dieterich* [1978, 1979], since adopted to varying degrees by others, is that the friction evolution effect arises from an inverse relationship between strength and slip rate, due to some velocity-dependent change in the physical state of the slip surface or gouge layer. For example, the average size of a population of asperity contacts may decrease upon an increase in slip rate, because less time is available for indentation creep to occur at the asperity contacts [*Dieterich*, 1978; *Dieterich and Kilgore*, 1994]. This explanation suggests that the evolution effect will act in a sense opposite to that of the direct effect (i.e., b_2 will be positive). Negative values of b_2 have been reported for room-temperature slip of carbonates (calcite, dolomite, magnesite-bearing serpentinite); however, those observations may reflect creep accommodated by dissolution and reprecipitation (L. Reinen, written communication, 1996) and are likely unrelated to the large values of b_2 reported here.

In Figure 7 we represent the dependencies of a and b_1 on temperature with lines separated by abrupt breaks in slope (heavy gray lines). This depiction matches our intuition regarding the micromechanical processes active during slip. For example, if we associate the direct effect with subcritical crack growth [*Lockner*, 1998], then the pronounced rise of a above 250° (Figure 7a) might reflect a switch in the rate-limiting step for that mechanism. Similarly, if we accept that time-dependent indentation creep gives rise to the evolution effect [*Dieterich and Kilgore*, 1994], then the change in slope of b_1 at 350° (Figure 7b) may reflect a change in the deformation mechanism that accommodates indentation.

Intuition is less helpful in guiding a continuous representation for parameter b_2. The transition temperature for b_2 marks a change in both the sign and magnitude of b_2 and a pronounced increase in D_{c2}. The evolutions of strength fitted by the second state variable at lower temperatures seem unrelated to those fitted by the same state variable in the hydrothermal regime. On this basis we argue that these processes are distinct and are represented by the same parameters only because of the nature of the constitutive laws assumed. (In essence, we are arguing for the use of a third state variable; however, the limitations in both the data and our understanding of the sliding process preclude our taking such a leap here.) We speculate that the process responsible for the large, negative b_2 operates over a wide range of temperatures but is only resolvable at temperatures above ~350° at these sliding rates, though alternative interpretations are possible.

Curiously, for velocity steps modeled with large, negative values of b_2, the associated evolution distance, D_{c2}, is much higher for upward velocity steps than for downward steps (Figure 7f). Visual inspection of the friction-displacement curves (Figure 2) suggests that poor resolution and subjectivity in detrending are not the sole causes of this bias, which is most pronounced when the slip law is used (Table 2). An interesting possibility is that the strengthening process quantified by the second state variable evolves not only with slip, but also with time. In this case the greater amount of time associated with slip at the lower rate would allow greater evolution toward steady state. Some slip dependence clearly remains; otherwise the ratio of the values of D_{c2} would be that of the slip rate contrast, 10, rather than roughly two. We have not attempted to model these data using state evolution laws which include time dependence; however, *Weeks and*

Tullis [1985] modeled friction data for dolomite using two state variables, one evolving with slip, the other evolving with time.

3.4. Stability of Sliding

Both sliding experiments and stability theory suggest that that unstable fault slip is promoted by velocity weakening and that stable fault slip is promoted by velocity strengthening. Small values of a and D_{ci} should also promote unstable slip. In this light, our results suggest that natural fault slip at modest rates should be stable (i.e., aseismic) at hydrothermal conditions, but may be unstable (i.e., seismic) at lower temperatures, lower pore fluid pressures, and/or high slip rates. Wet granite shows velocity weakening from 90°C to 350°C, so unstable slip may be possible at those temperatures, depending on the compliance of the mechanical system loading the fault. This range of temperatures is roughly consistent with the depth range of seismicity on mature faults in the continental crust [*Marone and Scholz*, 1988; *Blanpied et al.*, 1991].

Good correspondence exists between the stability of sliding observed in the granite experiments and the constitutive parameter values determined by inversion. For both wet and dry granite gouge, a tendency for unstable sliding was shown by oscillatory sliding (e.g., 150° and 200° wet, 200° dry) and small stick-slip events following upward steps in velocity (e.g., 300° wet, 273° dry). A dry test at 200° and wet tests at 200° and 225°C exhibited oscillations that could not be stabilized through adjustments to the servo-control system parameters. Thus ~200°C represents an approximate minimum in stability for slip at these laboratory rates. This temperature corresponds to the most negative values of a-b_1-b_2 as well as small a, large b_1, and small D_{c1}, each of which tends to destabilize sliding [e.g., *Gu et al.*, 1984; *Tullis and Weeks*, 1986]. At temperatures above the "transition temperature," stable sliding is promoted by large, positive values of a-b, large a, and large D_{c1}. These influences are more pronounced for wet than for dry granite. Furthermore, the negative values of b_2 for wet granite should inhibit unstable sliding by inducing rate strengthening and protracted strength transients. An experiment in which temperature was raised in increments of 50° (Figure 13) illustrates that crossing this transition can stabilize slip. Sliding at 200°C was oscillatory, consistent with results shown earlier (Figure 2). Heating to 250° reduced the magnitude of oscillations, and heating to 300° stabilized the sliding.

4. Conclusions

We have analyzed rate-stepping friction tests on granite to measure parameters in friction constitutive laws over a wide range of temperature and fluid pressure conditions. The experiments span a range of temperatures up to 845°C for dry granite gouge and up to 600°C with pore water pressure. We inverted the friction-displacment data to determine parameters for three alternative rate- and state-dependent friction constitutive formulations in the literature. This study was not designed to formally distinguish between the quality of fit attained by the three laws; each gave reasonable fits to the experimental data.

The inversion results depend on the constitutive law used, on the scheme used to detrend the data, and on whether we inverted individual rate steps or entire friction tests containing several steps. The experiments were run to small total displacement, so friction transients caused by slip rate steps were superimposed on hardening or softening trends. Thus the choice of detrending method was important. We found it best to apply a linear detrending to each rate step individually. The subjective choice of trend affects most strongly the values of parameters b_2 and D_{c2}. Some of the scatter in D_{c2} is clearly due to this.

Most steps from dry experiments were adequately fitted using a single state variable, as were those from wet experiments at the lowest temperature. Steps from wet experiments at higher temperatures required two state variables. For wet runs above 350°C the value of b_2 was large and negative, and the value of D_{c2} was large (several hundred to several thousand microns). The large value of D_{c2} meant that steady state was not achieved between velocity steps in those runs; in a few cases we inverted the entire set of velocity steps at once in order to deal with this difficulty. These whole-experiment fits provide an opportunity to directly compare the performance of the three constitutive laws. The con-

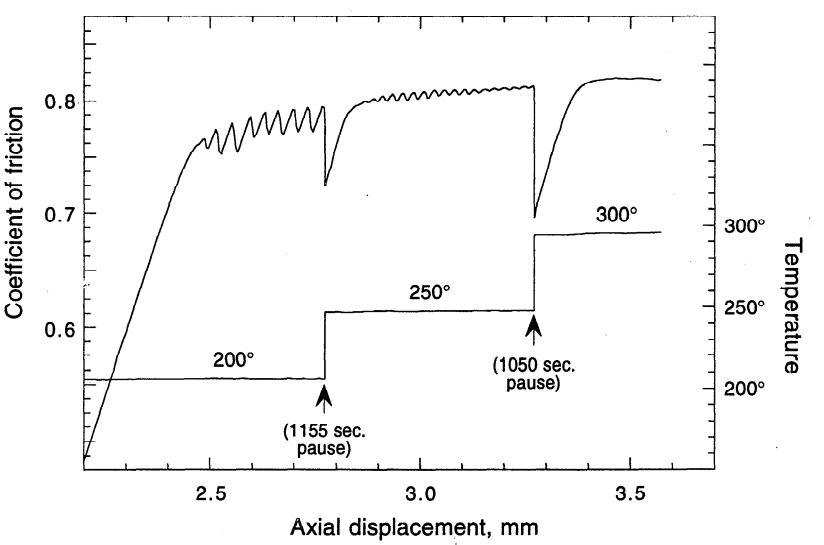

Figure 13. A sliding experiment on wet granite gouge illustrating the effect of temperature on sliding stability. Conditions are slip rate, 1 μm/s; effective normal stress, 400 MPa; and P_p = 100 MPa. Loading rate was set to zero for the time intervals indicated while temperature was raised in 50° increments. Sliding at 200°C resulted in oscillatory slip (periodic, aseismic oscillations of stress and slip rate). Raising temperature to 250° reduced the amplitude of the oscillations, and raising it to 300° stabilized slip.

stitutive laws proposed by *Ruina* [1983] (slip law) and *Perrin et al.* [1995] (quadratic law) provide similar, and adequate, fits to most rate steps. The formulation of *Dieterich* [1979] (slowness law) performs less well in matching the evolution of friction toward steady state, in agreement with previous studies. At hydrothermal conditions the protracted approach to steady state displays an asymmetry with respect to the sense of the velocity change, which is not reflected in any of the three laws. This asymmetry is reflected in the value of D_{c2} and implies that the evolution has a time-dependent element.

We plotted parameter values against inverse temperature to highlight trends. The decision to plot against inverse temperature is based on our assumption that the parameters quantify the rate of thermally activated deformation micromechanisms. The rate of those mechanisms presumably varies with temperature according to Arrhenius relationships. However, since we have not identified particular mechanisms or demonstrated that the parameters are linked to a particular rate law, we do not identify an activation energy. Each of the parameters a, b_1, and b_2 for wet granite shows a pronounced change in trend that may reflect a change of dominance of the underlying deformation mechanisms. These changes occur at transition temperatures T_T of roughly 270° to 350°C and may reflect the activation of fluid-aided processes.

We have quantified trends in the parameter values for the slip law (equations (2) and (3)) by two-segment linear regressions (Figure 7 and Table 5). These regressions provide a means to incorporate the full constitutive response of granite into numerical models of fault slip in the continental crust. We provide values for wet granite up to 600°C, applicable to a range of depth from the surface to considerably below the seismic-aseismic transition (generally 400° to 450°C for continental crust) [*Blanpied et al.*, 1995]. For those interested only in the steady state velocity dependence of friction we also provide a three-segment representation of the variation of $\partial\mu_{ss}/\partial V$ with inverse temperature. A susceptibility for unstable sliding is thought to correlate with velocity weakening, which in our three-segment representation is the case between 90° and 360°C. However, the details of the sliding behavior, including whether slip is stable or unstable, depend on the full constitutive description as well as the loading conditions.

Appendix: Long-Term Trends in Strength

We considered two alternative methods to determine the value of the detrending parameter C: choosing a single trend to best represent the overall rate of work hardening over many steps and choosing a separate trend for each velocity step. Data from three velocity steps are fitted using both methods (Figure 14). The parameters b_2 and D_{c2}, which describe the long-term evolution toward steady state, are particularly sensitive to the choice of trend. Note that both the magnitude and the sign of the velocity dependence can depend on the method used and our subjective choice of trends. For example, in the third step illustrated, the first method gives $a\text{-}b_1\text{-}b_2 = +0.008$, while the second method, using a much shallower trend, gives $a\text{-}b_1\text{-}b_2 = -0.002$. Because the rate of hardening decreases with slip in many experiments (e.g., Figure 1, 130° and 370°C), we found in using the first method that a single, linear trend was an inadequate representation and frequently gave bad fits. For this reason the second method was used to obtain the

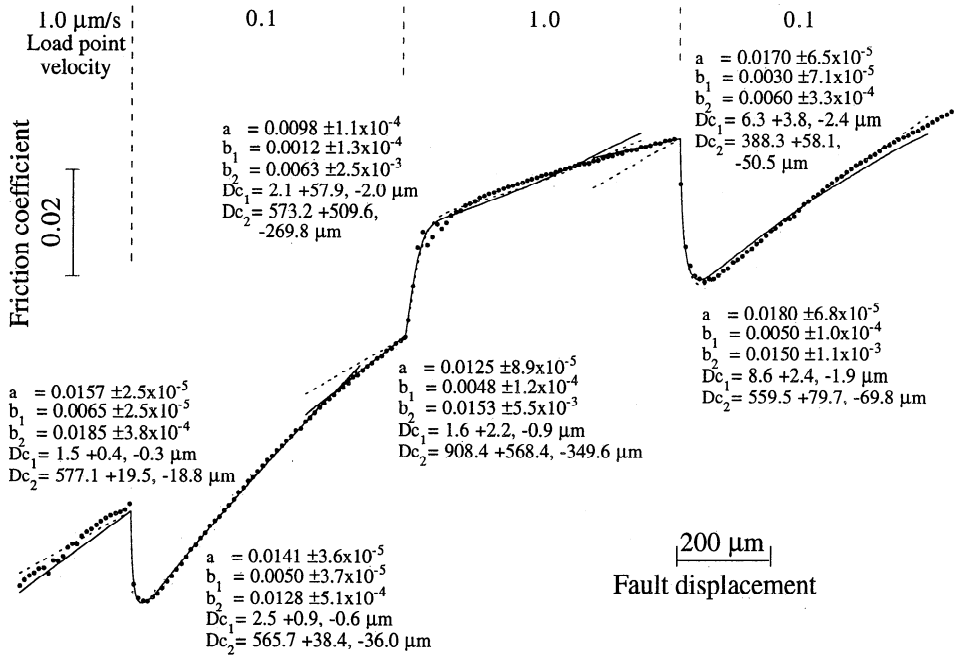

Figure 14. Data (dots) for three velocity steps at 250°C on wet granite gouge. Every tenth point is shown at the slower slip rate, while all points are shown at the faster rate. The response to each velocity step is fitted with the slip law, equations (2) and (3), and shown as dashed and solid curves. The response to velocity steps is superimposed on a significant work hardening trend, which we account for by adding a linear term to equation (2) (see text); the straight-line segment preceding the velocity step shows the detrend used for each simulation. We illustrate two alternative methods for choosing the value of the detrending term. In the first case (dashed curves) we chose a single trend (5.0×10^{-5} μm^{-1}) to best represent the overall rate of work hardening, and we used this value in the fit to each step. Parameters obtained in this case are listed above the data. In the second case (solid curves) we chose a separate trend for each step (6.5×10^{-5} μm^{-1}, 7.0×10^{-5} μm^{-1}, and 2.0×10^{-5} μm^{-1}, in order of increasing slip). Parameters obtained in this case are listed below the data.

fits to individual steps (as shown in Figures 5 and 6 and Tables 2 and 3). A third option is to detrend as in the first method, but using a higher-order function of displacement in place of $C\delta$. For a few experiments we tried polynomial functions of order 3 and 4 and obtained results that were similar to the second (piecewise linear) method. While this might be the most appropriate method, the data in most cases do not allow us to define such a function with any confidence.

Acknowledgments. This work benefited from discussions with N. Beeler, L. Reinen, and J. Weeks and reviews by M. Olsen, A. Leger, B. Hacker, N. Beeler, and L. Reinen . We thank L. Reinen and J. Weeks for sharing their computer program RWIM and advice in its use, and F. Chester for providing manuscripts in advance of publication. Funding was provided by the USGS Programs in Earthquake Hazards Reduction and Deep Continental Studies.

References

Beeler, N. M., T. E. Tullis, and J. D. Weeks, The roles of time and displacement in the evolution effect in rock friction, *Geophys. Res. Lett.*, *21*, 1987-1990, 1994.

Beeler, N. M., T. E. Tullis, M. L. Blanpied, and J. D. Weeks, Frictional behavior of large displacement experimental faults, *J. Geophys. Res.*, *101*, 8697-8715, 1996.

Ben-Zion, Y., and J. R. Rice, Slip patterns and earthquake populations along different classes of faults in elastic solids, *J. Geophys. Res.*, *100*, 12,959, 1995.

Biegel, R. L., C. G. Sammis, and J. H. Dieterich, The frictional properties of simulated gouge having a fractal particle distribution, *J. Struct. Geol.*, *11*, 827-846, 1989.

Blanpied, M. L., D. A. Lockner, and J. D. Byerlee, Fault stability inferred from granite sliding experiments at hydrothermal conditions, *Geophys. Res. Lett.*, *18*, 609-612, 1991.

Blanpied, M. L., D. A. Lockner, and J. D. Byerlee, An earthquake mechanism based on rapid sealing of faults, *Nature*, *358*, 574-576, 1992.

Blanpied, M. L., D. A. Lockner, and J. D. Byerlee, Frictional slip of granite at hydrothermal conditions, *J. Geophys. Res.*, *100*, 13,045-13,064, 1995.

Byerlee, J., Friction of rocks, *Pure Appl. Geophys.*, *116*, 615-626, 1978.

Chester, F. M., Temperature and rate dependence of friction for faults (abstract), *Eos Trans. AGU*, *69*, 471, 1988.

Chester, F. M., Effects of temperature on friction: Constitutive equations and experiments with quartz gouge, *J. Geophys. Res.*, *99*, 7247-7262, 1994.

Chester, F. M., A rheologic model for wet crust applied to strike-slip faults, *J. Geophys. Res.*, *100*, 13,033-13,044, 1995.

Chester, F. M., and N. G. Higgs, Multimechanism friction constitutive model for ultrafine quartz gouge at hypocentral conditions, *J. Geophys. Res.*, *97*, 1859-1870, 1992.

Dieterich, J. D., Time-dependent friction and the mechanics of stick-slip, *Pure Appl. Geophys.*, *116*, 790-806, 1978.

Dieterich, J. D., Modelling of rock friction, 1, Experimental results and constitutive equations, *J. Geophys. Res.*, *84*, 2161-2168, 1979.

Dieterich, J. D., Constitutive properties of faults with simulated gouge, in *Mechanical Behavior of Crustal Rocks (The Handin Volume)*, *Geophys. Monogr. Ser.* vol. 24, edited by N. L. Carter *et al.*, pp. 103-120, AGU, Washington, D. C., 1981.

Dieterich, J. H., A model for the nucleation of earthquake slip, in *Earthquake Source Mechanics*, *Geophys. Monogr. Ser.*, vol. 37, (Maurice Ewing Vol. 6), edited by S. Das *et al.*, pp. 37-47, AGU, Washington, D. C., 1986.

Dieterich, J. H., A constitutive law for rate of earthquake production and its application to earthquake clustering, *J. Geophys. Res.*, *99*, 2601-2618, 1994.

Dieterich, J. H., and B. D. Kilgore, Direct observation of frictional contacts: New insights for state-dependent properties, *Pure Appl. Geophys.*, *143*, 283-302, 1994.

Fredrich, J., and B. Evans, Strength recovery along simulated faults by solution transfer processes, in *Proceedings of 33rd U.S. Symposium on Rock Mechanics*, pp. 121-130, A.A. Balkema, Santa Fe, N. M., 1992.

Gu, J.-C., J. R. Rice, A. L. Ruina, and S. T. Tse, Slip motion and stability of a single degree of freedom elastic system with rate and state dependent friction, *J. Mech. Phys. Solids.*, *32*, 167-196, 1984.

Higgs, N. G., Mechanical properties of ultrafine quartz, chlorite and bentonite in environments appropriate to upper-crustal earthquakes, Ph.D. dissertation, 267 pp., Texas A & M, College Station, Tex., 1981.

Karner, S. L., C. Marone, and B. Evans, Laboratory study of fault healing and lithification in simulated fault gouge under hydrothermal conditions, *Tectonophysics*, *277*, 41-55, 1997.

Linker, M., and J. Dieterich, Effects of variable normal stress on rock friction: Observations and constitutive equations, *J. Geophys. Res.*, *97*, 4923-4940, 1992.

Lockner, D. A., A generalized law for brittle deformation of Westerly granite, *J. Geophys. Res.*, in press, 1998.

Lockner, D. A., and J. D. Byerlee, Laboratory measurements of velocity-dependent frictional strength, *U. S. Geol. Surv. Open File Rep. 86-417*, 1986.

Lockner, D. A., and J. D. Byerlee, Dilatancy in hydraulically isolated faults and the suppression of instability, *Geophys. Res. Lett.*, *21*, 2353-2356, 1994.

Lockner, D. A., R. Summers, and J. D. Byerlee, Effects of temperature and sliding rate on frictional strength of granite, *Pure Appl. Geophys.*, *124*, 445-469, 1986.

Marone, C., and B. Kilgore, Scaling of the critical slip distance for seismic faulting with shear strain in fault zones, *Nature*, *362*, 618-621, 1993.

Marone, C., and C. H. Scholz, The depth of seismic faulting and the upper transition from stable to unstable slip regimes, *Geophys. Res. Lett.*, *15*, 621-624, 1988.

Marone, C., C. B. Raleigh, and C. H. Scholz, Frictional behavior and constitutive modeling of simulated fault gouge, *J. Geophys. Res.*, *95*, 7007-7025, 1990.

Marone, C. J., C. H. Scholz, and R. Bilham, On the mechanics of earthquake afterslip, *J. Geophys. Res.*, *96*, 8441-8452, 1991.

Menke, W., *Geophysical Data Analysis: Discrete Inverse Theory*, Academic, San Diego, Calif., 1989.

Moore, D. E., D. A. Lockner, and J. D. Byerlee, Reduction of permeability in granite at elevated temperatures, *Science*, *265*, 1558-1561, 1994.

Morrow, C. A., and J. D. Byerlee, Experimental studies of compaction and dilatancy during frictional sliding on faults containing gouge, *J. Struct. Geol.*, *11*, 815-825, 1989.

Olsen, M. P., C. H. Scholz, and A. L_ger, Healing and sealing of a simulated gouge under hydrothermal conditions: Implications for fault healing, *J. Geophys. Res.*, in press, 1998.

Perrin, G., J. R. Rice, and G. Zheng, Self-healing slip pulse on a frictional surface, *J. Mech. Phys. Solids*, *43*, 1461-1495, 1995.

Press, W. H., B. P. Flannery, S.A Teukolsky, and W. T. Vetterling, *Numerical Recipes in C*, 818 pp., Cambridge Univ. Press, New York, 1988.

Reinen, L. A., and J. D. Weeks, Determination of rock friction constitutive parameters using an iterative least-squares inversion method, *J. Geophys. Res.*, *98*, 15937-15950, 1993.

Reinen, L. A., T. E. Tullis, and J. D. Weeks, Two mechanism model for frictional sliding of serpentinite, *Geophys. Res. Lett.*, *19*, 1535-1538, 1992.

Rice, J. R., and J.-C. Gu, Earthquake aftereffects and triggered seismic phenomena, *Pure Appl. Geophys.*, *121*, 187-219, 1983.

Ruina, A. L., Friction laws and instabilities: A quasi-static analysis of some dry frictional behavior, Ph. D. dissertation, Brown Univ., Providence, R. I., 1980.

Ruina, A. L., Slip instability and state variable friction laws, *J. Geophys. Res.*, *88*, 10,359-10,370, 1983.

Segall, P., and J. R. Rice, Dilatancy, compaction, and slip instability of a fluid infiltrated fault, *J. Geophys. Res.*, *100*, 22,155-22,171, 1995.

Sleep, N. H., Ductile creep, compaction, and rate and state dependent friction within major fault zones, *J. Geophys. Res.*, *100*, 13,065-13,080, 1995.

Stesky, R. M., The mechanical behavior of faulted rock at high temperature and pressure, Ph.D. thesis, 197 pp., Mass. Inst. of Technol., Cambridge, 1975.

Stesky, R. M., Mechanisms of high temperature frictional sliding in Westerly granite, *Can. J. Earth Sci.*, *15*, 361-375, 1978.

Stuart, W. D., Forecast model for great earthquakes at the Nankai Trough subduction zone, *Pure Appl. Geophys.*, *126*, 619-641, 1988.

Tse, S. T., and J. R. Rice, Crustal earthquake instability in relation to the depth variation of frictional slip properties, *J. Geophys. Res.*, *91*, 9452-9472, 1986.

Tullis, J., and R. A. Yund, Hydrolytic weakening of experimentally deformed Westerly granite and Hale albite rock, *J. Struct. Geol.*, 2, 439-451, 1980.

Tullis, T. E., The effect of pore fluid chemistry on the friction of quartz gouge, in *Proceedings of Workshop LXIII: The Mechanical Involvement of Fluids in Faulting*, edited by S. Hickman et al., *U. S. Geol. Survey Open File Report, 94-228,* 509-513, 1994.

Tullis, T. E., and J. D. Weeks, Constitutive behavior and stability of frictional sliding of granite, *Pure Appl. Geophys.*, *124*, 384-414, 1986.

Weeks, J. D., and T. E. Tullis, Frictional sliding of dolomite: A variation in constitutive behavior, *J. Geophys. Res.*, *90*, 7821-7826, 1985.

M. L. Blanpied, J. D. Byerlee, and D. A. Lockner, U. S. Geological Survey, 345 Middlefield Road, MS-977, Menlo Park, CA 94025. (e-mail: mblanpied@usgs.gov, dlockner@usgs.gov)

D. P. King and C. J. Marone, Department of Earth, Atmospheric and Planetary Sciences, Massachusetts Institute of Technology, Cambridge, MA 02139. (e-mail: cjm@westerly.mit.edu)

(Received April 22, 1997; revised December 9, 1997; accepted January 9, 1998.)